International Journal of Disaster Risk Reduction 121 (2025) 105403

Contents lists available at ScienceDirect

International Journal of Disaster Risk Reduction

journal homepage: www.elsevier.com/locate/ijdrr

High-resolution multi-hazard residential buildings and population exposure model for coastal areas: A case study in northeastern Italy

Hazem Badreldin [a,b,*], Chiara Scaini [a], Hany M. Hassan [a,b], Antonella Peresan [a]

[a] National Institute of Oceanography and Applied Geophysics, OGS, Via Treviso 55, 33100, Udine, Italy
[b] National Research Institute of Astronomy and Geophysics, NRIAG, 1 Marsad Street, Helwan, Cairo, Egypt

ARTICLE INFO

Keywords:
Multi-risk
High resolution exposure datasets
Census data
Residential buildings
Building footprints
Replacement cost

ABSTRACT

Developing high-resolution multi-hazard exposure models significantly improves risk assessment and loss estimation. In the present study, we propose and verify a methodology for developing a high-resolution exposure model for population and residential buildings that could be used for multi-hazard risk mitigation at the local scale across the globe. The methodology is applied to Lignano municipality, a coastal area located in the northern Adriatic, prone to multiple hazards such as seismically-induced tsunamis, meteorological events, coastal erosion and subsidence. The population exposure layer is developed integrating population data with demographic characteristics and socio-economic indicators. In parallel, the building exposure layer, which combines census data with digital building footprints, contains information about: geographic distribution, age of construction or retrofit, number of storeys, construction material types, average built-up area, structural replacement cost, and structural regularity. These data layers are made available at two resolutions: 100 m and 30 m, with information also provided at the census unit level. We describe the methodology developed for exposure assessment and discuss its potential use for multi-hazard risk assessment in coastal areas.

1. Introduction

Exposure modeling is paramount for disaster risk mitigation and reduction. Characterizing exposed assets is a required step in order to identify potential damages and losses and develop better risk mitigation strategies. However, exposure assessment is a complex task itself, as the exposed assets are dynamic, interrelated and contribute differently to the overall damages/losses. Past efforts in the field were focused on assessing exposure independently for different hazardous phenomena, depending on their spatial scales (e.g. floods, [1]; earthquakes, [2,3]). Few studies have developed multi-hazard exposure models, which have been used for multi-risk assessments (e.g., [4,5]). However, multiple hazards can occur simultaneously or consecutively [6], with cascade and amplification effects, which often increase expected impacts and risks (e.g., [7,8]).

Current efforts in the research community are devoted to combining the existing knowledge on single hazard and their impacts to account for potential occurrence of multiple hazards [9]. This is particularly relevant in coastal areas prone to land and marine geohazards occurring at different timescales (e.g. tsunami and meteotsunami [10], subsidence, floods, drought and coastal erosion

* Corresponding author. National Institute of Oceanography and Applied Geophysics, OGS, Via Treviso 55, 33100, Udine, Italy.
E-mail address: hbadreldin@ogs.it (H. Badreldin).

https://doi.org/10.1016/j.ijdrr.2025.105403
Received 12 August 2024; Received in revised form 13 March 2025; Accepted 14 March 2025
Available online 18 March 2025

[11]. Revised exposure classification systems and taxonomies are being developed to support the interoperability and combination of existing datasets at global and regional scales (e.g. GED4ALL by [12]) and are being refined at the national scale to account for specific contexts (e.g., [2]). In addition, characteristics deemed relevant for assessing vulnerability to a given phenomenon can play different roles in the response to different hazards [13]. For example, height can be a critical parameter, with tall buildings being more or less vulnerable to certain earthquake ground motion, but potentially life-saving in case of floods and tsunamis, besides other factors. Moreover, in today's urban landscape many buildings are designed with irregularities [14] which can increase their vulnerability in case of hazardous phenomena such as earthquakes [15]. In the case of floods, irregular building designs can disrupt water flow, make buildings more vulnerable to damage, and create uneven water pressure or lateral load on the structure. This, in turn, could increase the potentiality of a building experiencing structural failure [16]. For all these reasons, multi-hazard risk assessment methods require as accurate as possible high-resolution, up to date, and as much as possible realistic and validated exposure models.

Furthermore, modeling future exposure is increasingly important due to climate change, population growth, and the increasing urbanisation of societies [3,17, 18, 19]. However, combining the available sources of exposure datasets (e.g., census, ancillary data, building footprints) into high-resolution exposure layers poses some challenges [20]. Nowadays, there are few examples of high-resolution exposure layers that account for characteristics deemed relevant for multiple hazards (e.g., [21] and [22]). In addition, exposed assets monetary value is rarely available despite its relevance for associating and comparing financial exposure to multiple hazardous phenomena (e.g., [23]). Some exposure-related information contained in building footprints is still somehow overlooked and could enhance current exposure layers (for example, with relation to buildings area and shape factors). Some studies have demonstrated the effectiveness of openly available datasets in constructing exposure models for seismic and multi-hazard risk assessment. For example, Nievas et al. [24] and Gómez Zapata et al. [25] utilized OpenStreetMap [26] data for scenario-based seismic risk assessment, while Geiβ et al. [27,28] and Arrighi et al. [29] explored exposure modeling using satellite imagery and multi-hazard contexts, providing valuable insights relevant to this study.

There have been few efforts to investigate the uncertainties related to exposure composition (e.g., [30–33]). However, uncertainty in exposure models, which arises from assuming fixed proportions over aggregated data, greatly impacts risk analysis and loss estimation. Furthermore, various sources of uncertainty in an exposure model should be examined during risk analysis, such as the classification of buildings into different typologies and their spatial distribution [34].

In this work, we propose and introduce a methodology to develop high-resolution exposure assessment of urban areas, to be used for multi-hazard risk reduction purposes at a city or municipality scale. The methodology comprises extracting geometric information from footprints and integrating them into existing exposure layers, achieving higher spatial resolution and enhancing the description of exposed assets characteristics. Given that the data used in this work has been collected in almost every nation across the globe, we can assume the current methodology can be applied to other coastal areas worldwide. We demonstrate the approach for a selected coastal area located in the upper Adriatic, prone to multiple hazards such as seismically-induced tsunamis, meteorological events, coastal erosion and subsidence. We collect available data at local, national and global levels, both from official sources (e.g. building census) and open source or access datasets, focusing on population and residential buildings. The methodology leverages local-scale data, i.e. building footprint to develop indicators associated with building regularity and area, relevant for multi-hazard coastal exposure and loss assessment. The developed datasets shall support the definition and testing of multi-hazard risk assessment and the prioritization of action (e.g., targeted data collection) for resilient land use planning in the study area. We also discuss the potential application of the methodology in other areas with different characteristics, underlining its advantages and limitations.

This paper comprises two main parts: part one illustrates the materials, data, process and methods that have been used to develop high resolution population and residential building exposure models; part two provides a case study for a selected coastal area located in the Northeast of Adriatic, namely the municipality of Lignano Sabbiadoro.

2. Materials, data preparation, and methods

Multi-hazard disaster risk analysis requires combining exposure information developed at different spatial resolutions and scales (i.e. global, regional, national, local). The spatial resolution of exposure data, which is often aggregated at a broader scale and lower resolution, may not be comparable with the spatial variability and extent of certain hazards affecting coastal areas (e.g. tsunamis, floods, landslides, and coastal erosion). This variability depends on many factors, which are related, besides to data and hazard modeling limitations, to the physical nature of the hazard itself (e.g. flooding and tsunami inundation strongly depends on details of local scale topography). Therefore, if we aim to develop an exposure layer suitable for multi-risk assessment, we should target a spatial resolution as high as the variability of the most detailed considered hazard. For instance, tsunami hazard maps are already available at 25m resolution for the Northern Adriatic coasts (see Peresan and hassan, MEGR 2024), which justifies improving exposure resolution at 30m scale. Failing to get a sufficiently high-resolution exposure layer, clearly depending on available input data, may result in inaccurate risk assessment (both underestimation and overestimation).

Hence, addressing this mismatch between hazard and exposure assessments is essential for improving the precision and reliability of risk evaluations. Moreover, different vulnerability-related analyses may require specific information about individual buildings and their spatial distribution. For instance, when assessing exposure to earthquakes, gathering information on building materials and lateral load-resisting systems is key for achieving high spatial resolution risk estimates. However, for floods and tsunamis, knowing the height of the ground floor above ground level, occupancy of the ground floor, ground floor hydrodynamics and the number of storeys below ground level at a high-resolution is essential [1,35,36]. When dealing with population, the key factors influencing an individual's vulnerability to specific hazards include: age, income, health or disability status, and education [37]. These factors play a critical role in determining an individual's or household's ability to manage and respond to various impacts of hazards. The key

hazard-specific parameters and potential indicators of vulnerability for residential building and population are listed in Table 1. To tackle these challenges for coastal areas we present a comprehensive overview of the data collection, data preparation, tools and methods to be followed to develop high-resolution exposure models for population and buildings located in areas subject to multi-hazard.

2.1. Materials: exposure datasets

In this work, three different geospatial datasets are used to develop high-resolution population and residential buildings exposure models: national census of population and buildings, global population datasets and building footprints. These datasets contain exposure-related information relevant for possible application for coastal areas multi-risk analysis, including earthquakes, tsunamis, floods, landslides, and coastal erosion.

The geospatial datasets collected, processed and ingested in this work are:

2.1.1. National census data

National census data depending on the country, includes information on population and residential buildings. These data are always aggregated at a given spatial resolution, ranging from province or municipality level to smaller census units. National census data is considered as a detailed overview of a nation's population, building typologies, demographics distributions in space at a specific snapshot in time, and socioeconomic attributes. Globally, buildings are typically classified based on factors such as construction or retrofit age, material type, height, and occupancy. Meanwhile, population data is generally categorized by age and gender. These classifications play an essential role in defining the vulnerability of both buildings and populations to various hazards. Census data is gathered through a systematic process of counting and data collection, typically carried out every decade. It is available for most countries either at a local scale, through national censuses, or at a global scale, such as the Global Exposure Model [44].

2.1.2. High-resolution population density data

High resolution population density data, such as the one provided by Data for Good (part of the Meta company) for the year 2020 and lastly updated in April 2023. This dataset (hereinafter referred to as Meta data for ease of reference) contains high-resolution Population Density Maps at a 30-m pixel resolution (https://dataforgood.facebook.com/dfg/) [45], and was developed by the Center for International Earth Science Information Network (CIESIN), using artificial intelligence-AI to identify buildings based on satellite imagery. This granular data has significant implications for various fields, including urban planning, humanitarian aid, risk and emergency management and public health. This data is globally available and regularly updated.

2.1.3. Building footprints datasets

Building footprints datasets are increasingly used to develop high-resolution exposure layers. Globally, there are many resources for these digital building footprints, such as OpenStreetMap [26] (https://www.openstreetmap.org/). However, OSM only provides spatial distribution and geometry, lacking information on occupancy type and height, and potentially missing some data [46]. Land use maps, such as CORINE land cover data [47], can provide occupancy information. Different techniques have been developed to extract building height from aerial images [1] and other characteristics (e.g., occupancy types, construction types) from vertical satellite images [20,48]. Volunteered geographical information-VGI or/and crowdsourcing data can also support the collection of attributes

Table 1
Key hazard-specific exposure parameters and potential indicators of vulnerability.

Exposed asset	Feature	Hazard	References
Population	Age Education Income	Earthquake; Tsunami; meteo-tsunami; Flood	[23,35,37]
Residential buildings	Material	Earthquake	[12,38]
		meteo-tsunami; Tsunami	[37,39]
		Flood	–
	Age	Earthquake	[12,38]
		meteo-tsunami; Tsunami	[37,40]
		Flood	[41]
	Height/Number of storeys	Earthquake	[12]
		meteo-tsunami; Tsunami	[37,40]
		Flood	[42]
	Height regularity	Earthquake	[12,38]
		Tsunami; meteo-tsunami	[16,40]
		Flood	[42]
	Plan regularity	Earthquake	[12,38]
		Tsunami; meteo-tsunami	[16,40]
		Flood	[37]
	Replacement cost	Earthquake	[12,23]
		Tsunami; meteo-tsunami	[23,40]
		Flood	[23,43]

associated with building footprints and various vulnerability related parameters (e.g., [49–51]). Moreover, if digital building footprints are available from national scale datasets, which include more detailed information on buildings, they can be also used. This methodology guarantees a thorough and precise description of urban landscapes, integrating both authoritative and community-generated information.

The exposure dataset for residential buildings is complemented here with building costs per square meters, which are used to estimate the replacement cost. Additionally, in other regions, the value of buildings can be estimated using local expert judgments (e.g., Central Asia, [23]). These exposure datasets were developed by enhancing census data with complementary additional datasets. This approach allowed for the disaggregation of the census data and the incorporation of missing information that were not provided in the original census.

2.2. Data preparation and methods

The main challenges related with combining exposure information are collecting available data, dealing with the missing data or uncertain sources and data ingestion [52,25]. Exposure assessment relies on various sources with different spatial resolutions and acquisition methods, adopting both top-down and bottom-up approaches [53]. Census data stands out as the most significant source for reliable population and building data, but they are often provided in aggregated form for data protection purposes [54] and lack certain attributes that could affect vulnerability.

To overcome this limitation, disaggregation is often employed to redistribute the aggregated population or buildings data at a higher resolution (e.g., [23,54]). Several input data including land use, nighttime lights and infrastructure, can be used as proxies for disaggregation, providing indicators of human presence [54]. Moreover, other data sources are used to extract some building features that are missing in the census building. Therefore, in this study, for the development of the population exposure model, the Meta high-resolution population density data, was complemented with the national population census data, assumed to be more reliable with respect to the global dataset. Also, the building census data was complemented with the additional attributes provided by the digital footprints dataset and population density is used as a proxy to disaggregate the buildings data. In both cases, high-resolution data were combined with lower-resolution ancillary data (e.g. official census). Hence, the final exposure layer for the residential

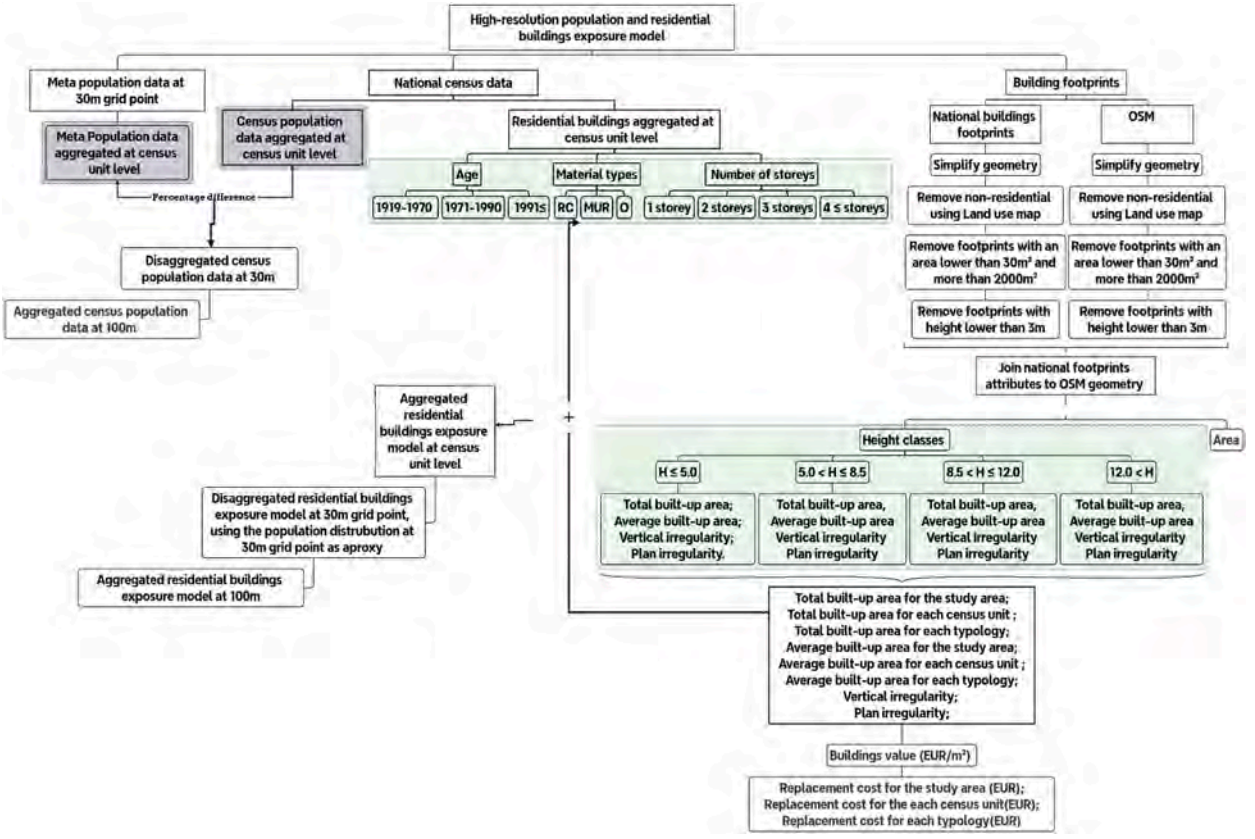

Fig. 1. Flowchart illustrating the development of high-resolution population and residential buildings exposure models. The green color indicates the two datasets (census residential buildings and building footprints) that have been used to develop the high-resolution residential buildings exposure model and grey color indicates the two datasets (the census population data and Meta population data) that have been used to develop the high-resolution population exposure model.

buildings is provided at a higher resolution than the census unit level (Fig. 1). All spatial operations are performed using the QGIS [55] open-source software. A step-by-step list of the Python libraries and QGIS [55] functionalities, all based on open-source code, *used in the spatial analysis workflow* is provided to ensure the replicability of the approach.

2.2.1. Population exposure layer

In the current work we present a methodology for development of high-resolution population exposure dataset by combining national and global datasets (see 2.1 for details), namely the Meta dataset (https://data.humdata.org/organization/meta) and the available census data. Meta data is available globally at 30-m grid points, while census data is aggregated at the census unit level. Census population data was used to refine the Meta data, combining the reliability of the census data with the higher resolution of the Meta data.

To achieve that, Meta data was aggregated to the same level as the census data. Consequently, the percentage difference (Pr_{diff}) between the national census and the Meta dataset can be estimated according to the below equation.

$$Pr_{diff} = \frac{(P_{census} - P_{Meta})}{(P_{census} + P_{Meta})/2} * 100 \quad (1)$$

Where P_{census} is census population number at the census unit, P_{Meta} is the Meta population number aggregated at the same census unit level. The comparison shall be also performed for each census unit, and the percentage difference can be used to correct the Meta dataset (Fig. 2) by it in each point of the Meta 30 m grid, by using equation (2).

$$corrected\ Meta\ population = \frac{DP_{Meta} * (Pr_{diff} + 200)}{(200 - Pr_{diff})} \quad (2)$$

DP_{Meta} refers to the Meta population dataset at a 30m grid point. The corrected Meta population now represents the disaggregating census population data to the same 30m grid, ensuring that when aggregated back to the census unit level, the total population matches exactly with the original census population for each unit.

The flowchart in Fig. 2 illustrates the disaggregation of census population data into a 30m grid using Meta data. In addition, a 100m grid has been developed by aggregating the 30m data grid as illustrated in Fig. 2. The demographic characteristics (e.g. age, gender, educational level, citizenship and employment status) were also disaggregated on the Meta grid using the same approach adopted for disaggregating the total population number. Based on the census data, the day occupancy was computed as total population number minus employed individuals, while night occupancy is assumed to match the population.

Seasonal variations in coastal populations pose significant challenges for accurate risk assessment and disaster response and are considered as a limitation in the current work. Traditional census data often fails to capture dynamic fluctuations, leading to underestimations of the population at risk during peak seasons. To address this, researchers and policymakers are exploring innovative approaches, such as real-time monitoring using mobile phone data and social media analytics, to estimate seasonal population fluctuations. By incorporating these dynamic estimates into exposure models and early warning systems, we can improve the effectiveness of disaster preparedness and response efforts in coastal regions.

2.2.2. Residential buildings exposure layer

The available residential buildings census data is categorized into many typologies, based on age, number of storeys and construction material types as mentioned in Section 2.1.1. Each census unit is characterized by a number of building classes, reflecting the

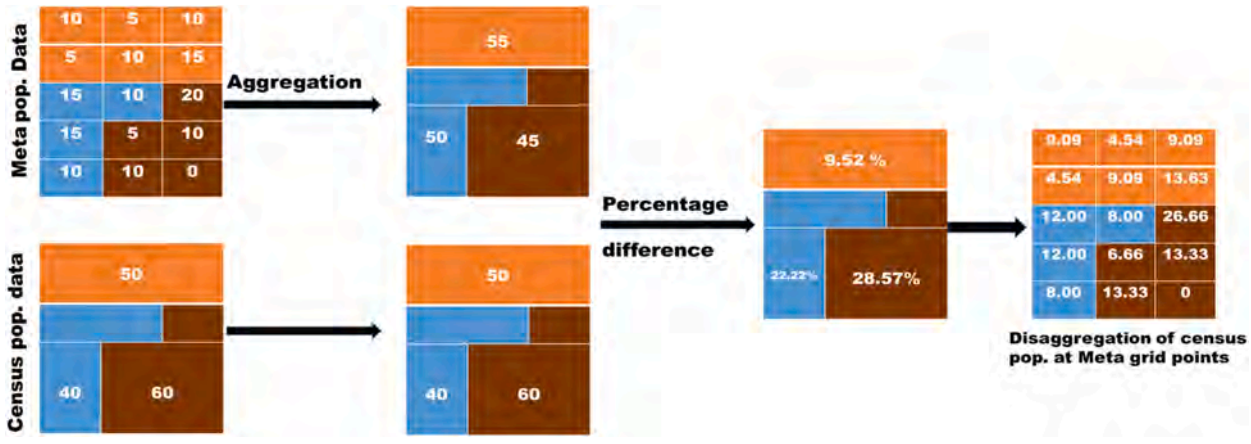

Fig. 2. A flowchart of the process used to disaggregate the census population data into a 30m regular grid using the Meta population data. Each color represents a different census unit. From left to right, the flowchart shows how the Meta data are aggregated at the census level resolution in order to compute the percentage difference, which is then applied to each cell of the high-resolution grid.

predefined typologies of the census buildings. In this study, building typologies were grouped and associated with the available vulnerability model classes in the literature, developed based on observed seismic fragility similarities [56].

The residential buildings exposure dataset in the proposed methodology is assembled by combining two data sources: the last updated building census data (section 2.1.1) and building footprints (section 2.1.3). The two datasets have different spatial resolutions (aggregated residential buildings at the census unit level versus single-building footprints) and different attributes. They nonetheless share information about building height, expressed in meters in the building footprints and number of storeys in census buildings. Building footprints dataset provide valuable information that is currently not accessible from official census data, such as area, height, spatial location, and occupancy type. Building's footprint-derived information was therefore assimilated into the census based on matching height classes. This is done under the assumption that some characteristics of civil buildings (in particular those related to their geometry) are homogeneous across height classes. This assumption enables us to associate characteristics derived from building footprints (e.g., average area) to the residential buildings stock in the same height range for each census unit. A sketch of the methodology is shown in Fig. 3.

The developed methodology consists of 3 steps: a) identification of height classes; b) extraction of building characteristics from footprints; c) integration of census and footprint characteristics into a high-resolution building exposure layer (30 and 100-m). Finally, the residential buildings reconstruction cost is also computed in each census unit. Each step of the methodology is described below.

2.2.2.1. Identification of height classes. Multiple attached footprints often represent a single building, so the geometries of attached footprints are simplified by dissolving them. Moreover, building footprints may also include non-residential structures (e.g., touristic,

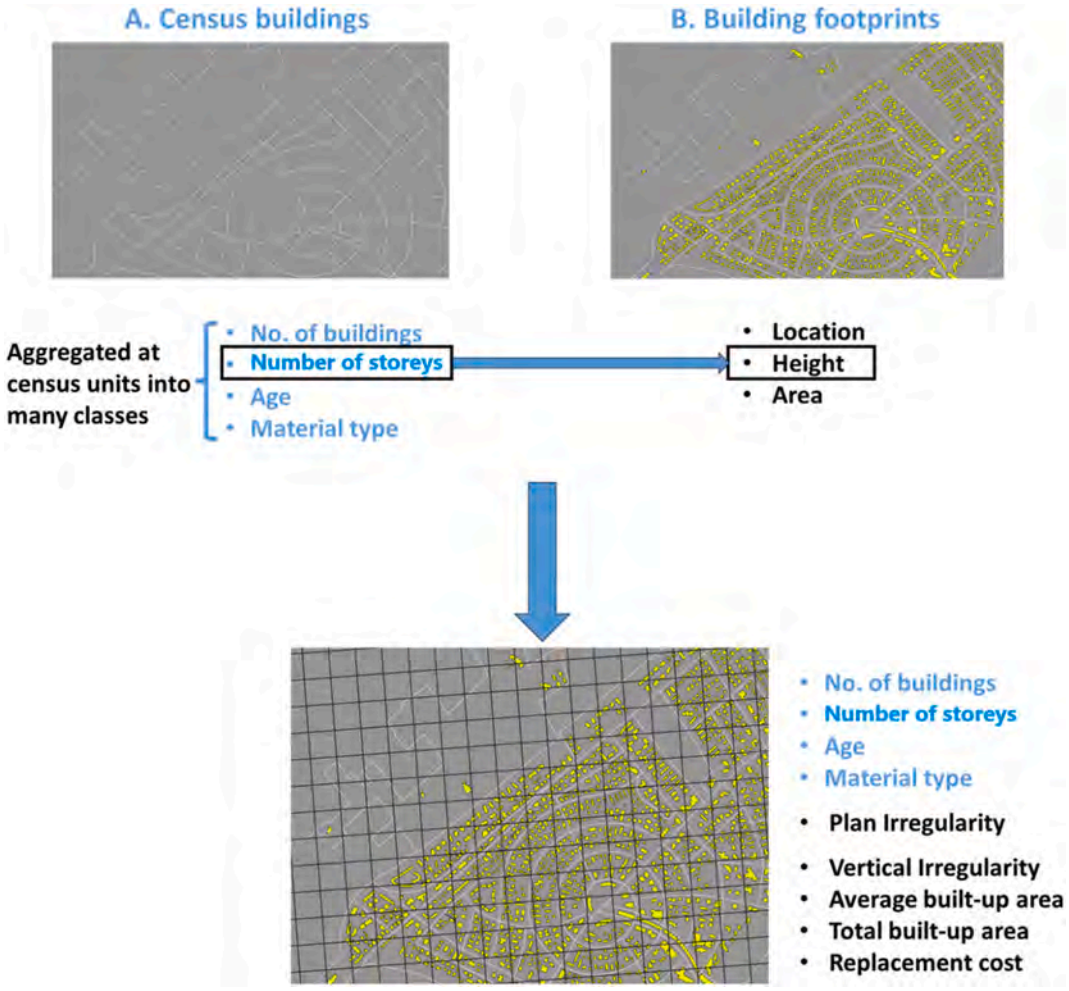

Fig. 3. The procedure for generating the high-resolution building exposure layer by integrating building footprints and census data. Census buildings (A) are aggregated at the census unit which represented by white polygons, while building footprints (B) are represented by yellow. The process involves classifying building footprints into height categories that align with the number of storeys in census data. Subsequently, building characteristics such as height, area, plan irregularity, and vertical irregularity are extracted from footprint data. These attributes are then merged with the aggregated census buildings for each storey class within each census unit and further disaggregated into a high-resolution building exposure layer at 30 m and 100 m resolutions.

commercial). Therefore, a land use map, along with specific area and height thresholds (i.e. 30 m^2 and 3m respectively), are applied to filter out non-residential buildings. Buildings in each census unit are classified based on the number of storeys into a set of classes. To align with this classification, building footprints are categorized into corresponding height classes ($H \leq 5.0m$; $5.0m < H \leq 8.5m$; $8.5m < H \leq 12.0m$; $H > 12.0m$) based on the number of storeys indicated in the census data class (1 storey; 2 storeys; 3 storeys; 4 ≤ storeys) (Fig. 1). This classification may vary from one area to another and should be validated to ensure accuracy with residential buildings.

2.2.2.2. Extraction of building characteristics from footprints. In this study, we compute average buildings area in each height class based on the footprints, and define new indicators to classify buildings based on their regularity in plan and in height.

- Average building area

For each height class the average building area is computed based on the footprint geometry. First, the average footprints area in each height class is calculated. Then, it is multiplied by the number of census buildings in the corresponding height class. The procedure is repeated for each census unit. Consistency checks can be run to identify potential underestimation or overestimation of built area.

- Plan Irregularity

Regarding the plan regularity, we tested three different methods to classify buildings based on their geometric characteristics. Shape ratio was calculated as.

- the ratio between the long and short edges of the minimum bounding rectangle of the building;
- the percentage difference between the area of the minimum bounding convex hull of the building footprints and the area of the building footprints;
- the percentage difference between the area of the minimum bounding rectangle of the building footprints and the area of the building footprints.

Using the shape ratio of the minimum bounding rectangle of the building footprints, all building footprints were found to have a value of less than 4. However, this is unrealistic compared to building footprints which also exhibit convex geometries. The percentage difference between the area of the minimum bounding rectangle and the area of the building footprints, all building footprints gave more reliable results and was validated against selected footprints. A threshold value of 10 % was defined and allowed to split the footprints between a dominant class of regular buildings and the irregular ones (Fig. 4). The percentage of regular and irregular buildings in each height class was computed in each census unit. Finally, the number of regular and irregular buildings in each census unit was estimated by applying the percentage to the number of census buildings in each corresponding height class.

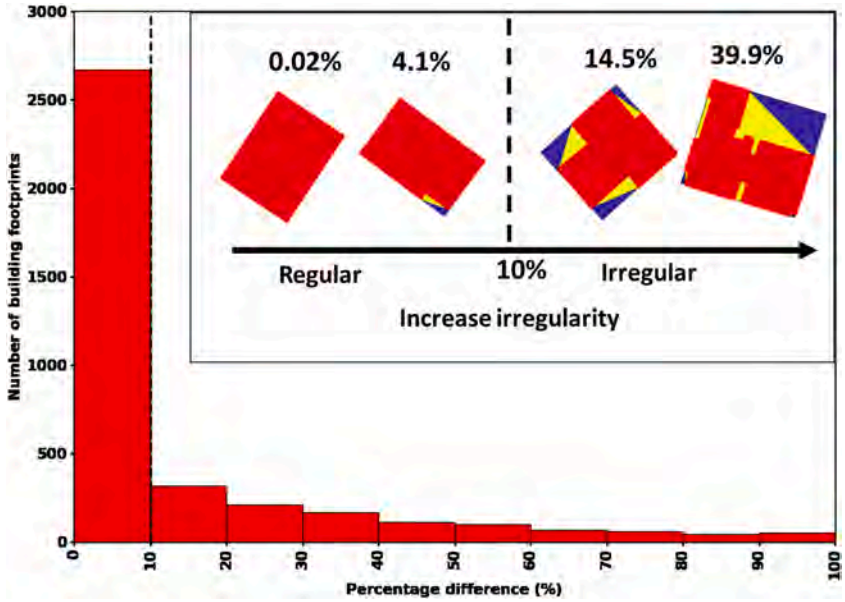

Fig. 4. Proposed classification for buildings plan regularity in the study area. Building footprints are classified based on the percentage difference between their area (red) and the area of the minimum bounding rectangle (blue), while the yellow color indicates the minimum bounding convex hull, which was tested but not used for the proposed classification.

- Vertical Irregularity

A building is characterized by vertical irregularity if one floor is significantly different in height from the others [57]. The indicator of vertical irregularity has been defined as the percentage difference between the maximum height and minimum height of the building footprints (both obtained from the dissolved footprints). Vertical irregularity was only assessed for footprints that contain the information about the minimum and maximum height; this is not available in OSM, but it can be derived from national footprint datasets such as the Italian CTRN (section 2.1) before dissolving them.

A threshold of 10 % difference between the maximum and minimum height is assigned to distinguish between vertically irregular and regular buildings (Fig. 5). The percentage of regular and irregular building footprints is estimated for each height class, similarly to what was done for plan regularity. The number of regular and irregular buildings was computed by multiplying the total building in each height class by the respective percentage. Most of the buildings in the study area exhibit vertical regularity (Fig. 5).

2.2.2.3. Integration of census data and footprint characteristics. The final high-resolution buildings layer is obtained by disaggregating buildings in each census unit using as a proxy the population distribution on a 30m regular grid. In a few census units, there are few residential buildings without a corresponding population. In such cases, the number of buildings was divided among the Meta grid points, assuming an equal distribution of buildings. The disaggregation was carried out independently for each height class. Information on age, number of storeys, material types, total built area, number of irregular and regular buildings in height and shape is also disaggregated (see equations (3) and (4)). The building exposure layer at the 30m grid is then aggregated to a 100m grid.

$$Pop_{weight} = (P_{30m} \,/\, P_{census}) \tag{3}$$

$$DB_{30m} = \left(Pop_{weight} * B_{census}\right) \tag{4}$$

where Pop_{weight} represents the proportion of the population at 30 m grid points (P_{30m}) relative to the total population within each census unit (P_{census}), while DB is the disaggregated building exposure model at 30m grid points, and B_{census} corresponds to the number of residential buildings within each census unit.

2.2.2.4. Replacement cost estimation. Replacement cost estimation is the process of determining the cost to replace a damaged building with a structurally equivalent building at current market prices. This involves considering factors such as construction costs, labor costs, material costs, permits, and other associated fees. Accurate replacement cost estimates are crucial for insurance claims, property valuations, and disaster recovery planning. By providing a realistic assessment of rebuilding costs, these estimates help property owners and insurers make informed decisions and allocate resources effectively.

This cost is usually given in local currency then can be transferred to one another per square meter for each residential building type in each area. Here, we assume that the building's reconstruction cost is equal to the market value. Each building value is computed multiplying the corresponding cost per square meter by the building area obtained from the footprints (equation (5)). This

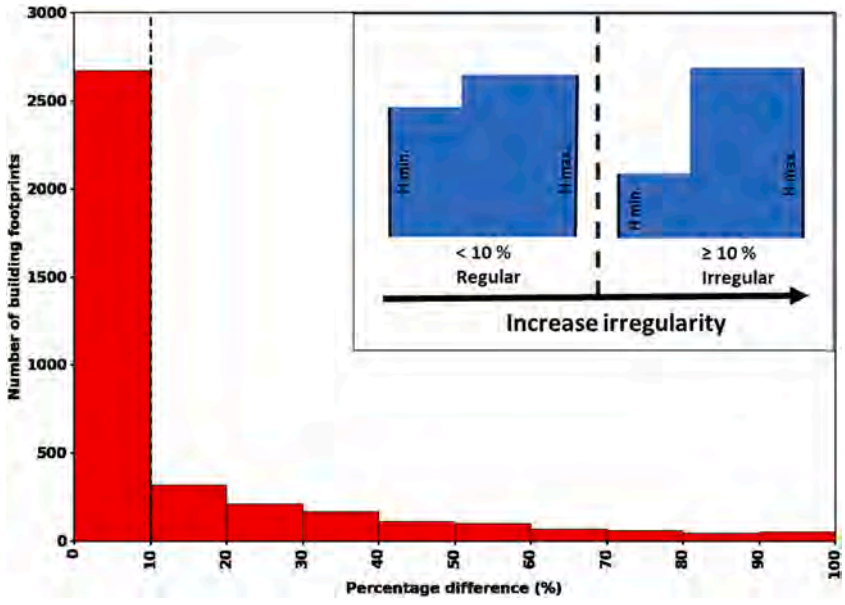

Fig. 5. Histogram shows the percentage difference between the maximum height and minimum height of building footprints used for estimating vertical regularity. A threshold of 10 % percentage difference was defined to classify buildings into regular and irregular.

computation is performed separately for each census unit of the final aggregated dataset. If building types with different values are present within the same census unit, the average is used.

$$Replacement\ Cost\ (EUR) = building\ value\left(EUR/m^2\right) * built-up\ area\ \left(m^2\right) \quad (5)$$

The final building's exposure layer contains the following parameters, which are deemed relevant for the coastal hazards: population number and its demographic; building material, age, number of storeys, structural regularity, and replacement cost.

3. Application and results

3.1. The study area

The Friuli-Venezia Giulia (FVG) region is located in northeastern Italy. Its coastal region, including the city of Lignano, situated on the northeast Adriatic Sea (Fig. 6), faces various land and marine natural hazards such as floods, powerful winds, coastal erosion, earthquakes, tsunamis, and meteotsunamis [58–60]. Given the vulnerability of these coastal areas, reducing the risks associated with these disasters is crucial for the social and economic development of the region. Lignano, in particular, is a major tourist destination, attracting several hundred thousands visitors during the summer. The considerable variability of the population throughout the year, and the presence of multiple hazards which could potentially affect Lignano, makes it an area of particular interest for creating as accurate as possible high resolution exposure models. Nowadays, the city has a population of approximately 6854 residents, with a notably higher population density in the urban core compared to the more suburban areas. Covering an area of about 15.71 square kilometers, the average population density comes to around 436.4 people per square kilometer [61]. Men represent 49.4 % of the population, whereas women comprise 50.6 %, resulting in a total of 3633 females [61].

The FVG region lies at the convergence of the Adria microplate and the Eurasian plate, at the junction between the Alps and Dinarides mountain systems. This complex seismotectonic setting is the primary reason for the high level of seismic activity in the region [62,63]. Throughout history, the region experienced a number of destructive earthquakes, the Friuli earthquake (M6.4) on May 6, 1976 [64] being the most recent destructive one, resulting in the deaths of 989 people [65]. On this occasion, most of the displaced population was temporarily relocated to the coastal area, in particular in Lignano [65]. Historical records also indicate that the Adriatic region experienced considerable impacts from earthquakes and tsunamis in the past [58–60]. However, while strong tsunamigenic earthquakes are infrequent in the Adriatic Sea [66,67], even moderate tsunamis can have undesirable effects due to the presence of sites of high historical, cultural, and touristic interest, as well as fragile ecosystems such as lagoons and river deltas.

In addition, the Adriatic Sea represents a hotspot for meteotsunamis, with destructive events every few decades [68–72]. Regarding flood hazards in the FVG region, the meandering part of the Tagliamento river can be subjected to flooding [73]. Finally, Lignano is exposed to sea level rise and is vulnerable to land subsidence due to its low elevation coastline with the highest subsidence rate among FVG region cities, approximately 4 mm/year [74]. Lignano was primarily developed after the 1950s, transforming a natural landscape of sand dunes, forests, and wetlands, similar to those still partially preserved on the opposite side of the Tagliamento River mouth. This historical transformation underscores the need to consider natural landscape preservation in future disaster risk reduction (DRR) plans. The socio-economic significance and the fact that various hazards affecting Lignano make it an excellent candidate for implementing the methodologies that have been developed.

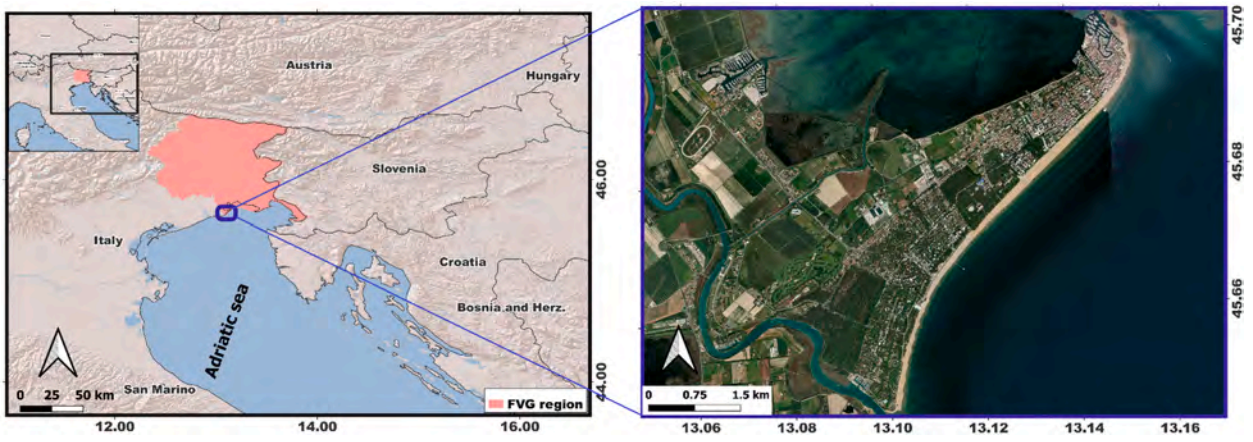

Fig. 6. Regional map for the FVG region, located in northeastern Italy (left panel) and aerial view of the Lignano municipality (right panel). Background map data extracted from Google maps(https://www.google.com/maps).

3.2. Available datasets

3.2.1. The national census data

The census data used in the current study for the Lignano area is extracted from the Italian National Institute of Statistics (ISTAT) and is shown in Fig. 7. The residential buildings data for the year 2011 [75] is used in this study, which is the last completed and updated buildings census data for Northeastern Italy [50]. It is aggregated at the census unit level, with the census unit area ranging from approximately 1800 m^2 in urban areas to 3.23 km^2 in rural areas. In this study, buildings are categorized into many typologies, based on the age (i.e. < 1919; 1919–1945; 1946–1970; 1970–1990; 1990–2005; >2005); number of storeys (i.e. 1 storey; 2 storeys; 3 storeys; 4 ≤ storeys); and construction material types (i.e. masonry; reinforced concrete; mixt from the other two types or other) [76].

The population census data is available for 2021 from the census database (Fig. 7) [61], which is providing detailed information about the Italian population, aggregated at the same census unit of the residential buildings. Different classes have been developed based on age (i.e. 0-5 to >74 years); gender (male, female), educational level (educated, not educated), citizenship (Italian, foreigners), number of families and employment status (employed, unemployed). The number of tourists in Lignano during the summer of 2023 reached 3,790,865 (https://www.promoturismo.fvg.it/it/89976/dati-istat-sul-turismo), most of whom stayed in residential buildings. However, there is no precise information available regarding the locations of these buildings to include in the final exposure model. Nonetheless, this data indicates a significant increase in population exposure during the summer months, which consequently amplifies the associated risks.

3.2.2. High-resolution global population dataset

High-resolution Population Density Maps at a 30m pixel resolution (https://dataforgood.facebook.com/dfg/) [45] was retrieved from Data for Good at Meta (hereinafter called Meta data for sake of easiness) (Fig. 8). In this work, we adopted the most recent available Meta dataset as of 2020, which was last updated in April 2023. Alongside overall population estimates, this dataset provides estimates for various demographic categories including overall population density, male, female, women of reproductive age, children, youth, and elderly. It is important to note that the Meta high-resolution dataset provides population estimates (see Section 2.1), rather than precise counts. Therefore, assessing its accuracy and adjusting it based on local or national data (as detailed in Section 2.2.1) is essential before utilizing the data for social exposure and vulnerability analyses.

3.2.3. Building footprints

The digital building footprints for the study area are derived from the [77] (CTRN, 2003) (https://eaglefvg.regione.fvg.it/) and [26] (OSM, 2022) (https://www.openstreetmap.org/). CTRN (2003) building footprints information about buildings' occupancy, area, and height are inferred from photogrammetric analyses; this detailed information is not always available in OSM building footprints. On the other hand, the geometry of OSM building footprints is more representative of the actual shape of buildings and does not require the geometric simplification seen in CTRN building footprints.

The last update of CTRN and OSM data for Lignano was in 2003 and 2022 respectively, which has been indicated from the last date of the building footprint images. The CTRN and OSM included all different types of buildings in the municipality of Lignano, but non-civilian footprints were excluded from the analysis. The CTRN (2003) was assembled by the FVG regional government based on photogrammetric analyses and we assume that these building footprints and the information contained hereby are reliable for the purpose of exposure development. The building footprints were also compared with the land use products in order to check their consistency.

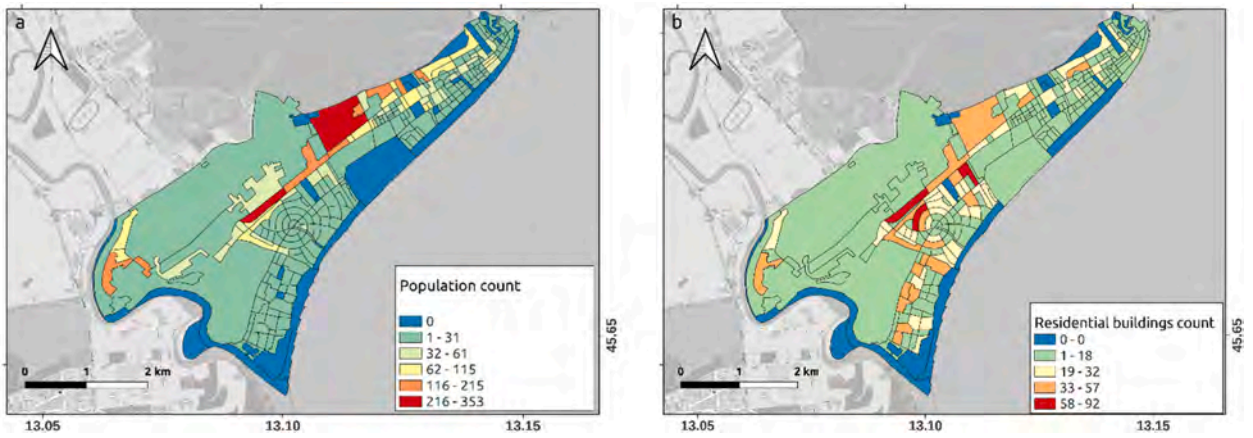

Fig. 7. Spatial distribution of the population counts for each census unit (left panel) [61]. Spatial distribution of the count of residential buildings in each census unit (right panel) [75].

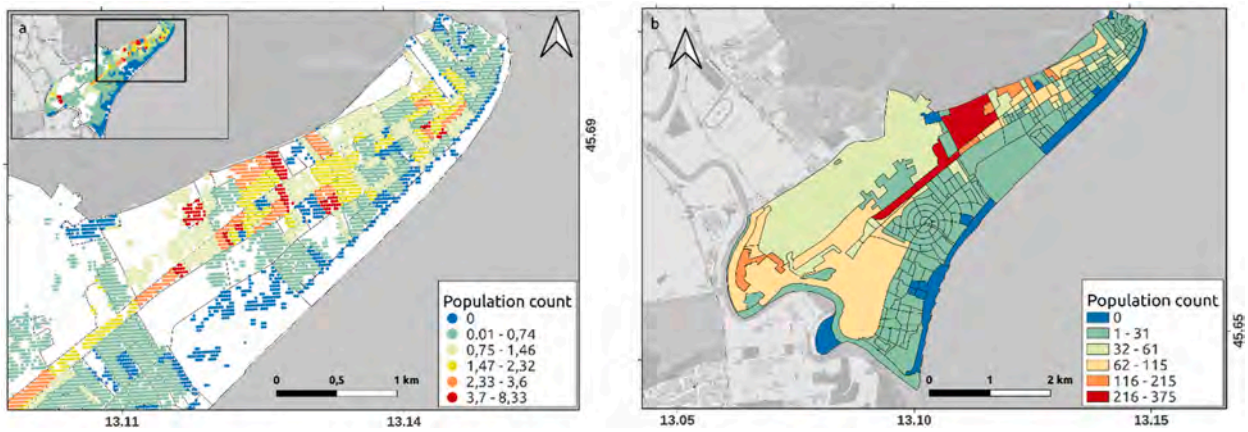

Fig. 8. Spatial distribution of the Meta population layer displayed on: a regular 30 m grid (left panel), and census unit level (right panel).

3.3. High-resolution population exposure layer for Lignano

The percentage difference between the national census and the aggregated Meta dataset is estimated, which is approximately 2 % at the Lignano municipality scale (Fig. 9). The estimated percentage difference used to refine the Meta population data at 30m grid. The developed population exposure layers are provided at 30m and 100m resolutions (Fig. 10). Population is classified based on its demographic characteristics (i.e. population grouped into many age classes, gender distribution, night and day occupancy and number of families) and socio-economic indicators (e.g. number of citizens, foreigners, employed individuals).

3.4. High-resolution residential buildings exposure layer for Lignano

The correspondence between number of buildings from census data and footprints is usually not exact (Fig. 11). This is because civil buildings footprints also include non-residential buildings (e.g. tourist, commercial). Also, multiple attached footprints often represent one single building. Geometries of attached footprints were therefore simplified prior to computing the height. The minimum and maximum height values were nonetheless retained from the individual footprints. The attributes of the CTRN (2003) building footprints have been joined to the geometry of the OSM building footprints. This approach was chosen because the latter database is more up-to-date, while the former provides more detailed information. However, the geometric simplifications in the CTRN (2003) building footprints could affect their accuracy. As a result, we utilized the geometry of the OSM building footprints, enriched with detailed information such as usage, minimum height, and maximum height derived from the CTRN (2003) building footprints. Nevertheless, some buildings that exist only in [26] (e.g. new buildings) contain only the area attribute. To mitigate the misfit between the two datasets, the footprints with an area lower than 30 m^2 and height lower than 3m (that could be related to garages or any non-residential buildings) were eliminated.

The buildings in each census unit are therefore classified using the height classes listed in Table 2, and associated with the corresponding characteristics derived from the footprints. This is achieved by estimating the percentage of building footprints for each

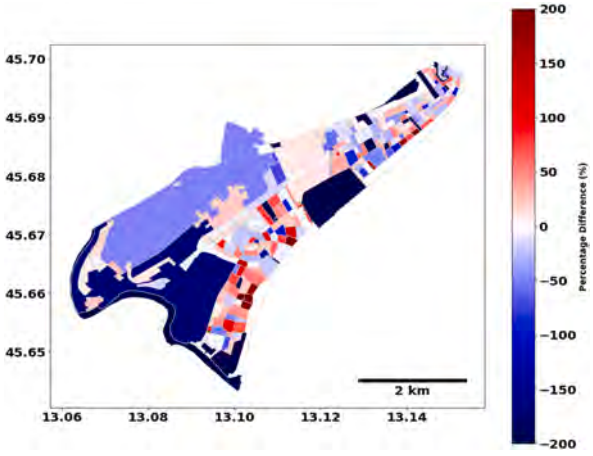

Fig. 9. The percentage difference between census population data and Meta population data for each census unit in the Lignano municipality.

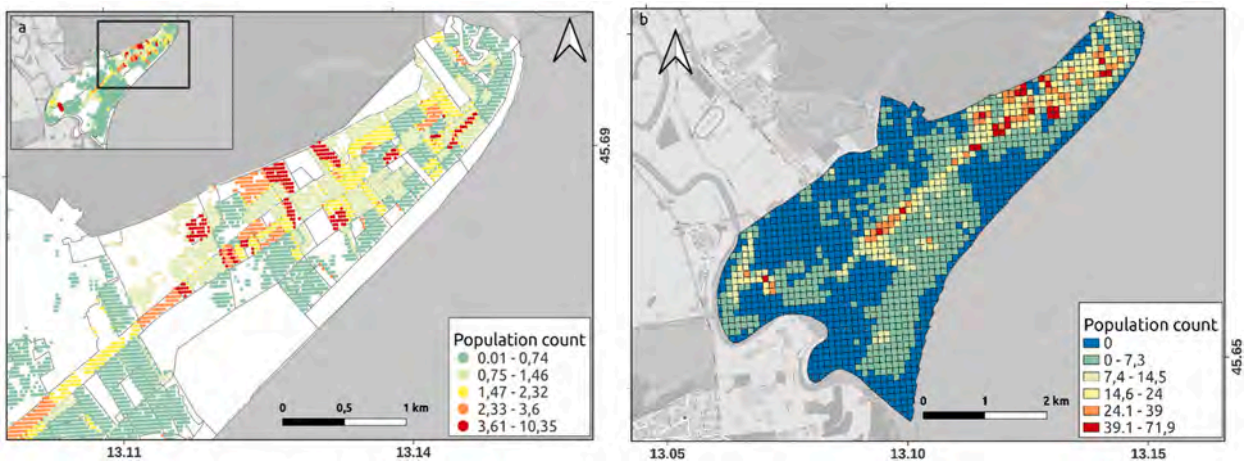

Fig. 10. Exposure layers produced for population [61], a) disaggregated on a regular 30 m grid and (b) aggregated on a 100 m regular grid.

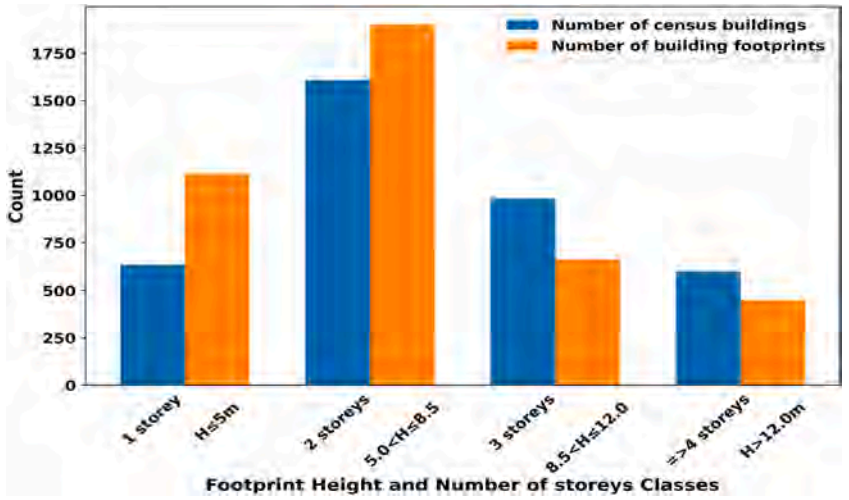

Fig. 11. Number of building footprints for each height class (H ≤ 5.0m; 5.0m < H ≤ 8.5m; 8.5m < H ≤ 12.0m; H > 12.0m), and number of buildings in each storey class (1 storey; 2 storeys; 3 storeys; 4 ≤ storeys).

Table 2
Building footprint height intervals and the corresponding storeys height in the census buildings for the Lignano municipality.

Building footprints height (m)	No. of storeys in the census buildings
H ≤ 5.0	1
5.0 < H ≤ 8.5	2
8.5 < H ≤ 12.0	3
12.0 < H ≤ 15.5	4
15.5 < H ≤ 19.0	5
19.0 < H ≤ 22.5	6
H > 22.5	>6

height class, and multiplying it by the number of census buildings in the corresponding height class.

Average built-up area for each height class in the building footprints is computed and multiplied by the number of census buildings in the corresponding height class (Table 1) to estimate the total built-up area. In the study area, only 2 out of 273 census units exceeded the percentage of built-up area of 90 % which is deemed unrealistic. This discrepancy arises from attached houses, which are represented as a single footprint in all footprint resources (e.g., OSM, CTRN), whereas the building census identifies them as multiple houses (Fig. 12). In these census units, the total built area was computed as the sum of all building footprints (assuming that they are all

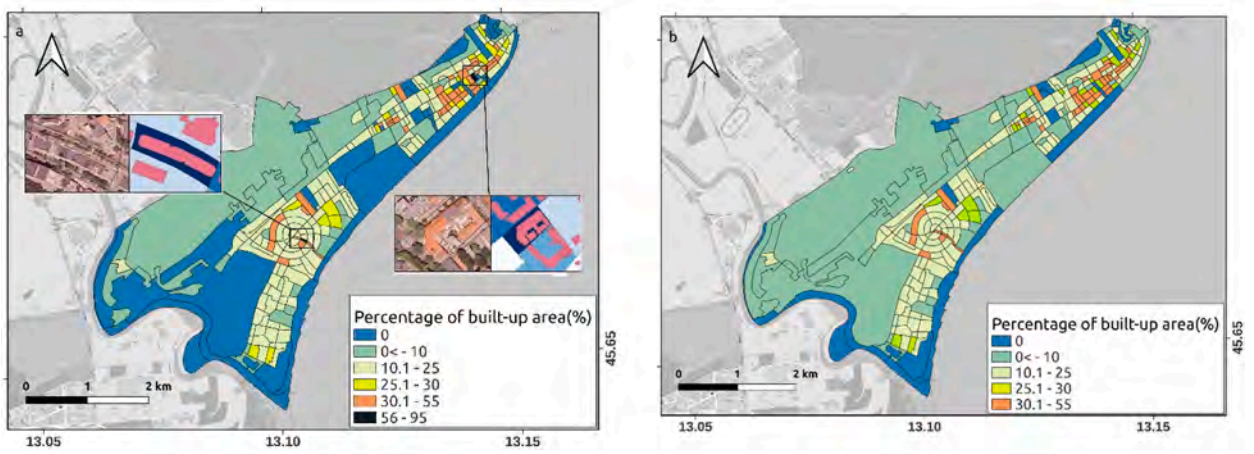

Fig. 12. Percentage of built area per census unit. Two methods are used to calculate this: (a) Multiply the average building area in each height class by the number of census buildings in that class. (b) Divide the sum of all building areas by the census unit area. This method (b) is only used for units where method (a) results in an unrealistic percentage over 90 %. Black polygons delimit the census unit.

residential). All other census units have a percentage of built area less than 55 % (Fig. 12). Fig. 13 displays, as an example, a map of structural regularity in building footprints within a specific area of the Lignano municipality, demonstrating that most buildings exhibit both plan and vertical regularity.

The developed residential building layer contains information about building age, number of storeys, construction material types, average built area, total built area, replacement cost, vertical regularity, and plan regularity, classified following the taxonomy in Table 3. The final residential building exposure layer is provided at three different resolution levels: census unit, 30m and 100m resolutions (Fig. 14). The replacement cost exposure layer is produced at the census unit level (Fig. 15). The total replacement cost for the municipality of Lignano is estimated at approximately 3 billion Euros. Mixed building materials, consisting of reinforced concrete and masonry, represent the highest total replacement cost, amounting to 1902.76 million Euros. This significant cost is attributed to the large number of buildings constructed with these materials and their substantial built-up area (Fig. 16).

4. Discussion and conclusion

The proposed methodology leverages available information on the selected coastal area and develops high-resolution exposure datasets for multi-hazard risk assessment. This is particularly relevant in areas prone to fluvial or pluvial floods or marine hazards, which present a high degree of spatial variability. The developed exposure layers are provided in three different forms: on 30m and 100m resolution grids and at the census unit level, combining information extracted from national census of population and buildings, and footprints datasets. However, Other resolutions can be developed based on the availability of the datasets and the end user request.

The methodology presented here can complement existing exposure datasets developed at the regional scale for Europe (e.g. [79]), which have lower spatial resolution and assume constant values of, e.g., built area. The exposure layers are developed using a well-defined multi-hazard taxonomy (GED4ALL Global Exposure Database for Multi-Hazard Risk Analysis; [12]) developed by the Global Facility for Disaster Reduction and Recovery (GFDRR). This taxonomy was complemented with a new, national-scale multi--hazard taxonomy developed by multi-Risk sciEnce for resilienT commUnities undeR a changiNgclimate (RETURN, [80]) and with new indicators to account for building geometric characteristics (see appendix A). In particular, we included new indicators for building plan and height irregularity which are derived directly from footprint data. We select thresholds (e.g. for height or plan regularity) that are context-dependent, so that they account for the actual geometric characteristics of buildings in the area. This allows to circumvent the uncertainty associated with using broader-scale typologies and derive regularity information that is relevant for assessing potential damages due to earthquakes (e.g. [81]; [82]), tsunamis [83] or both [84]. This study demonstrates the applicability of existing multi-hazard taxonomies and identifies potential features to be included. However, other features (i.e., occupancy of the ground floor, and number of storeys below ground) were not included in the current study due to the difficulty of retrieving such information. Including these features in the building exposure model (e.g. using field surveys) would provide a more realistic estimation of the building expected damages in case of occurrence of multiple hazards. Methods which are commonly employed in exposure analysis rely on the correlation between the number of buildings and population density [1,23]. Unrealistic exposure values can lead to inconsistent results, which were be verified by running spatial checks (e.g. on total built area in each census unit, Fig. 12) and by visual inspection, which was possible due to the relatively small extent of the area (see Appendix B). These checks allowed for the calibration of the exposure layer but ad-hoc verification and validation activities should be planned when applying the methodology to other areas.

The resulting spatial layer should therefore be used carefully due to the uncertainty that can be introduced by spatial operations (e.g. disaggregation) at the local scale, and are therefore not intended for single-asset exposure and risk assessment. Residual problems associated with missing or uncertain data might be tackled by involving local experts, e.g. practitioners, and validated with targeted

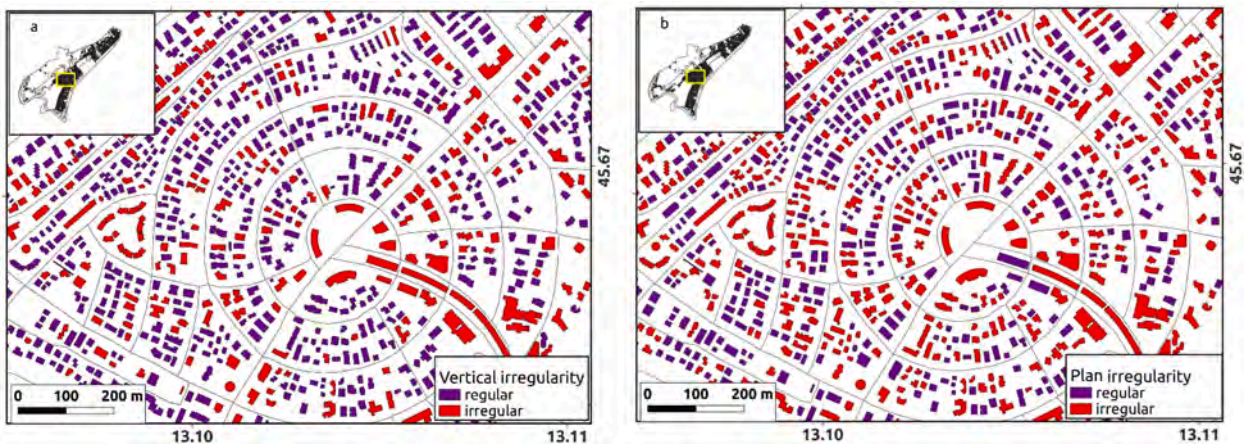

Fig. 13. Map showing the structure regularity/irregularity in the building footprints. Left panel shows plan irregularities, where building footprints are classified based on the percentage difference between their area and the area of the minimum bounding rectangle. Right panel shows vertical irregularities, where building footprints are classified based on the percentage difference between the minimum and maximum height.

Table 3
Building typologies and occupancy defined for residential buildings in Lignano, based on [61,75]. GED4ALL building taxonomy scheme has been used to write this taxonomy. The table also includes the built-up area for each taxonomy class, and the associated replacement cost.

Taxonomy	occupancy	Number of buildings	Built-up area (m^2)	Replacement cost (M EUR)
MUR/LWAL/HEX:1/YPRE:1971/RES	38.06	143.00	24989.67	68.44
MUR/LWAL/HEX:2/YPRE:1971/RES	191.72	265.00	54156.07	161.95
MUR/LWAL/HEX:3/YPRE:1971/RES	145.83	112.00	31849.16	98.78
MUR/LWAL/HBET:4-/YPRE:1971/RES	128.61	59.00	28502.49	93.10
MUR/LWAL/HEX:1/YBET:1980,1996/RES	19.59	80.00	10581.30	27.38
MUR/LWAL/HEX:2/YBET:1980,1996/RES	128.15	145.00	31114.15	85.43
MUR/LWAL/HEX:3/YBET:1980,1996/RES	42.51	45.00	11589.01	36.58
MUR/LWAL/HBET:4-/YBET:1980,1996/RES	69.57	28.00	14766.18	47.62
MUR/LWAL/HEX:1/YBET:1997,2011/RES	4.09	14.00	2149.94	5.42
MUR/LWAL/HEX:2/YBET:1997,2011/RES	33.92	21.00	4871.13	14.20
MUR/LWAL/HEX:3/YBET:1997,2011/RES	73.05	22.00	5900.86	17.42
MUR/LWAL/HBET:4-/YBET:1997,2011/RES	52.78	15.00	5930.79	19.96
CR/LINIF/HEX:1/YPRE:1971/RES	6.81	29.00	4033.18	11.91
CR/LINIF/HEX:2/YPRE:1971/RES	164.02	145.00	37121.84	111.05
CR/LINIF/HEX:3/YPRE:1971/RES	178.27	64.00	23043.96	65.98
CR/LINIF/HBET:4-/YPRE:1971/RES	159.86	46.00	25082.15	82.43
CR/LINIF/HEX:1/YBET:1980,1996/RES	6.71	17.00	2443.51	6.27
CR/LINIF/HEX:2/YBET:1980,1996/RES	45.53	42.00	8785.95	24.50
CR/LINIF/HEX:3/YBET:1980,1996/RES	273.07	87.00	29793.55	82.46
CR/LINIF/HBET:4-/YBET:1980,1996/RES	183.62	46.00	33886.85	97.72
CR/LINIF/HEX:1/YBET:1997,2011/RES	9.14	17.00	2658.06	7.37
CR/LINIF/HEX:2/YBET:1997,2011/RES	42.99	38.00	10678.52	29.84
CR/LINIF/HEX:3/YBET:1997,2011/RES	65.34	17.00	6299.37	16.83
CR/LINIF/HBET:4-/YBET:1997,2011/RES	102.09	16.00	6884.05	20.52
O/LWAL/HEX:1/YPRE:1971/RES	23.44	95.00	13733.95	36.94
O/LWAL/HEX:2/YPRE:1971/RES	290.40	286.00	64200.80	188.09
O/LWAL/HEX:3/YPRE:1971/RES	357.55	200.00	57636.86	186.35
O/LWAL/HBET:4-/YPRE:1971/RES	584.80	140.00	70060.49	221.39
O/LWAL/HEX:1/YBET:1980,1996/RES	60.75	177.00	28996.94	79.20
O/LWAL/HEX:2/YBET:1980,1996/RES	484.79	548.00	123587.85	329.02
O/LWAL/HEX:3/YBET:1980,1996/RES	657.17	311.00	95378.42	280.89
O/LWAL/HBET:4-/YBET:1980,1996/RES	895.60	183.00	93204.11	289.77
O/LWAL/HEX:1/YBET:1997,2011/RES	57.86	66.00	9850.69	27.73
O/LWAL/HEX:2/YBET:1997,2011/RES	319.44	119.00	28150.44	74.61
O/LWAL/HEX:3/YBET:1997,2011/RES	586.38	124.00	38056.40	104.71
O/LWAL/HBET:4-/YBET:1997,2011/RES	349.51	68.00	25977.06	84.02

crowdsourcing (as proposed by Scaini et al. [50,85]) currently being implemented in the study area. Also, the increasingly available spatial information data (e.g. high-resolution satellite and aerial images) can potentially support machine learning approaches (e.g. [20,86]) to complement the methodology described here. The methodology is calibrated for a coastal area in northeastern Italy exposed to different hazards, including earthquakes, fluvial and pluvial floods and marine hazards.

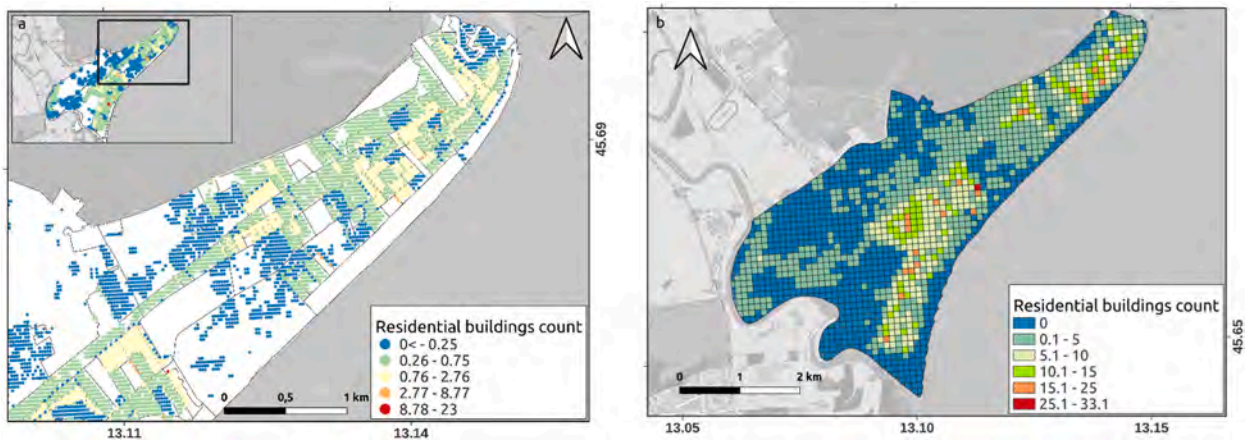

Fig. 14. Exposure layers produced for residential buildings, disaggregated on a regular 30 m grid (upper panel) and aggregated on a 100 m regular grid (lower panel).

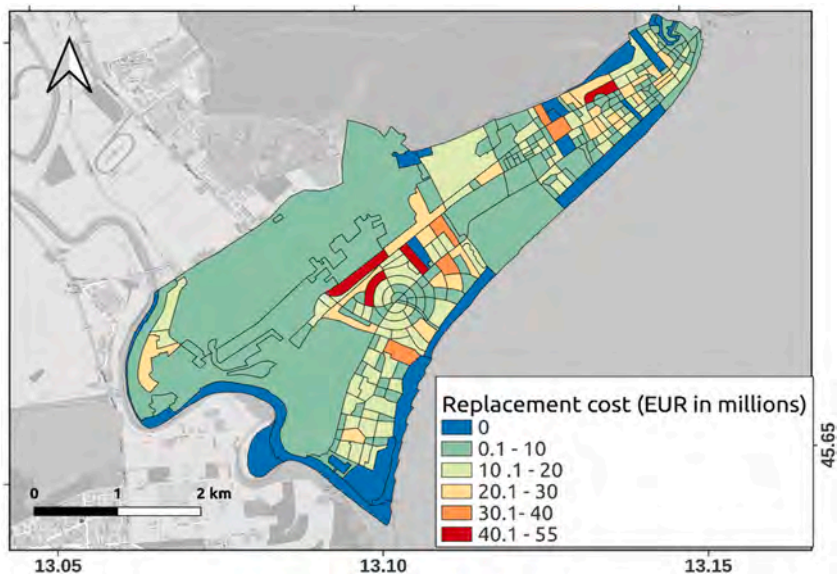

Fig. 15. Replacement cost of residential buildings at the census unit level, which is estimated using the built-up area and the building value for the year of 2023 [78].

5. Outlook

The case-study highlights the potential of the proposed methodology for further multi-hazard and multi-risk analyses, and allows discussing advantages, shortcomings and limitations of the approach. The proposed methodology can be adapted to be applied in data-scarce areas using remote-sensing to identify building footprints, and using lower-resolution census and ancillary data (e.g. [23]). Future work will focus on assessing and reducing uncertainties, in particular due to the availability and reliability of input data and the validity of the underlying assumptions (e.g. the proxies selected for spatial disaggregation). Preliminary verification of the obtained results is encouraging, but extensive testing and validation in different areas may provide important insights for further improving methodology and results.

Future work will also involve testing, validation and application of this methodology in other areas of the Mediterranean region which are exposed to multi-hazard (e.g. Alexandria city in Egypt, [87]), adapting it to diverse geographies, hazard types, and data availability constraints. Finally, we will actively engage school students through citizen science initiatives to extensively verify our findings and formally validate the proposed methodology, while enhancing their awareness and understanding [88].

As for the results of the case-study, the potential use of the developed layers was preliminarily discussed with selected stakeholders and end-users (e.g. municipality and civil protection representatives) at different resolutions depending on their requirements and the data policy. Higher resolution layers are not intended to be released publicly due to potential ethical issues, and their use is restricted to

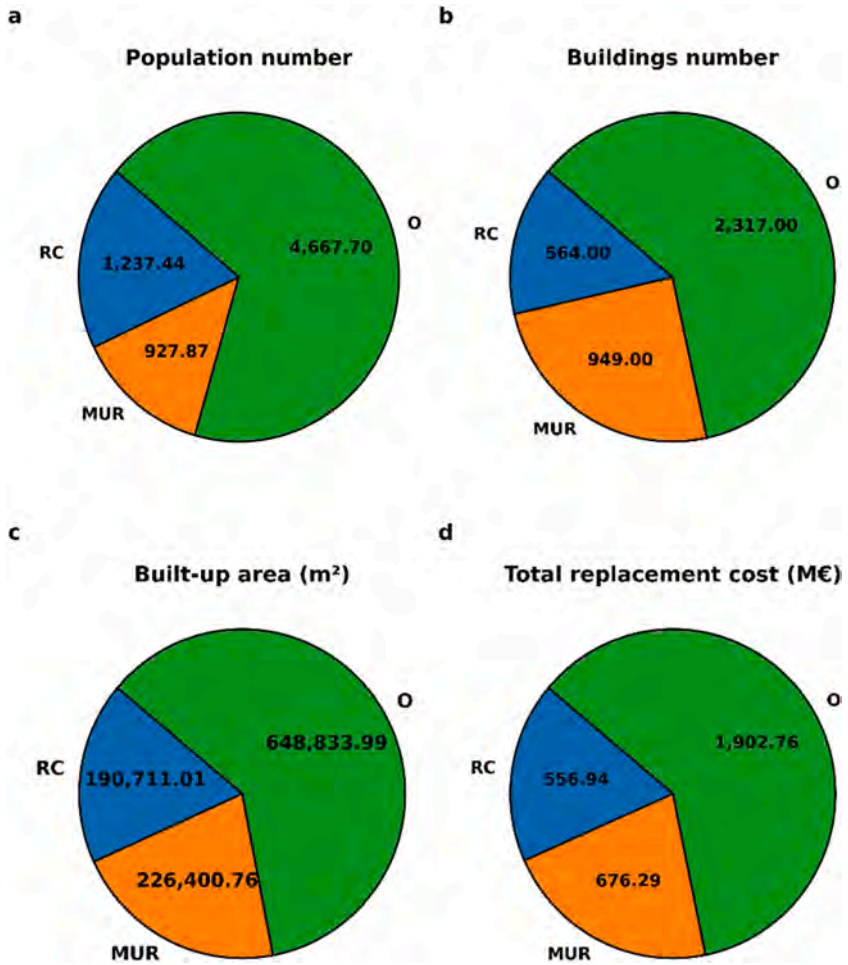

Fig. 16. Pie chart showing the distribution of population number , residential buildings number, built-up area, and replacement cost across the different building material types (i.e. masonry: MUR; reinforced concrete: RC; and mixt from the other two types or other: O) for the Lignano Municipality.

selected emergency managers such as the Civil Protection. The exposure dataset developed here is intended to be used in combination with hazard data, in particular from physics-based tsunami simulations (e.g. [66]), and vulnerability assessments to estimate risk and potential losses, inform disaster risk reduction activities (e.g. the design of evacuation plans) and support ecosystem-based land-use planning in riverine and coastal areas [89,90].

CRediT authorship contribution statement

Hazem Badreldin: Writing – original draft, Validation, Methodology, Formal analysis, Conceptualization. **Chiara Scaini:** Writing – review & editing, Validation, Methodology, Funding acquisition, Conceptualization. **Hany M. Hassan:** Writing – review & editing, Validation, Conceptualization. **Antonella Peresan:** Writing – review & editing, Validation, Supervision, Funding acquisition, Conceptualization.

Declaration of competing interest

The authors declare that they have no known competing financial interests or personal relationships that could have appeared to influence the work reported in this paper.

Acknowledgments

The study is a contribution to the RETURN Extended Partnership (European Union Next-Generation EU - National Recovery and Resilience Plan – NRRP, Mission 4, Component 2, Investment 1.3 – D.D. 1243 2/8/2022, PE0000005) and to the PRIN-PNRR project

SMILE: Statistical Machine Learning for Exposure development, funded by the European Union- Next Generation EU, Mission 4 Component 1 (CUP F53D23010780001).

Appendix A

Table A.1
Checklist table for building typologies and occupancy characteristics developed using the RETURN taxonomy [90]. A checkmark (✓) indicates a developed characteristic, while an (X) denotes an undeveloped characteristic that requires more data and field surveys for completion.

Attribute group	Attribute		method
Occupancy	Number of occupants	✓	Total population number
	Occupancy of ground floor	x	
	Daily/night	✓	Daily=total population number - employed individuals Night = Total population number
	Seasonal use	x	
	Cultural heritage asset	x	
	Age classes	✓	16 age classes
	Gender	✓	
	Number of families	✓	
	Employed	✓	
	Non-employed	✓	
	Italian and foreigners	✓	
Building Features	Age of Construction or age of retrofit	✓	1919–1970; 1970–1990, >1990
	Number of storeys	✓	4 storeys classes (1; 2;3; 4≤)
	Height of structure (m)	✓	Building footprints elevation + 1.5m
	Number of storeys below ground	x	
	Average plan surface	✓	Total built area and average built area from building footprints
Vertical structure system	Direction	x	
	Building Material type	✓	RC; URM; mixed-others
	Gravity load system	x	
	Lateral load coefficient	x	
	Ductility/quality	x	
	Lateral load resisting system	x	
	Seismic code level	x	
Building configuration and regularity	Building position in the block	x	
	Plan regularity	✓	Percentage difference between the area of the minimum bounding rectangle of the building footprints and the area of the building footprints
	Elevation regularity	✓	Percentage difference between the maximum height and minimum height
Building horizontal diaphragms	Floor type	x	
	Roof shape	x	
	Roof covering material	x	
	Roof system material	x	
Hydrological aspects	Height of ground floor above ground	x	
	Protection measures	x	
Foundation and soil condition	Foundation system	x	

Appendix B

Verification and preliminary validation activities were conducted in five target areas (approximately 50 buildings) within Lignano during July 2024. All authors visually inspected these areas and used OSM data to verify the developed method, ensuring coverage of diverse building typologies and ages. For details on the validation activities, see Appendix B. Irregularities/regularities in building plan and height were extensively checked at the five target areas. Most irregularities/regularities are correctly estimated using building footprints, except for: a) newly reconstructed buildings where mismatched footprints were found, b) hotels with long horizontal curtain coverage, causing vertical irregularities in the building footprints, and c) Some buildings are missing in the CTRN (2003) building footprints but are present in the OSM footprints. Therefore, their height irregularities could not be determined, as we relied on height differences to estimate it, which are only available in the CTRN 2003) footprints. However, plan irregularity was estimated using either OSM or CTRN footprints, as we only needed the footprint area which can be estimated easily using GIS.

Additionally, a number of new residential, touristic or mixed-use high-rise buildings with irregular shapes and often exceeding ten storeys, are currently under construction. In several cases, these new buildings are replacing older, low-rise single-family houses, and are not included in the census data and building footprints. These high-rise buildings, seismically-resistant, could be advantageous for vertical evacuation during floods or tsunamis, but they also have larger occupancy. Their presence should be therefore accounted for in

revised emergency plans. Some other areas are experiencing intensive expansion with the construction of new buildings, typically with two storeys. Some of these buildings were under construction during the validation activities in July 2024. So far, this expansion is not captured by the census data, OSM, and building footprints.

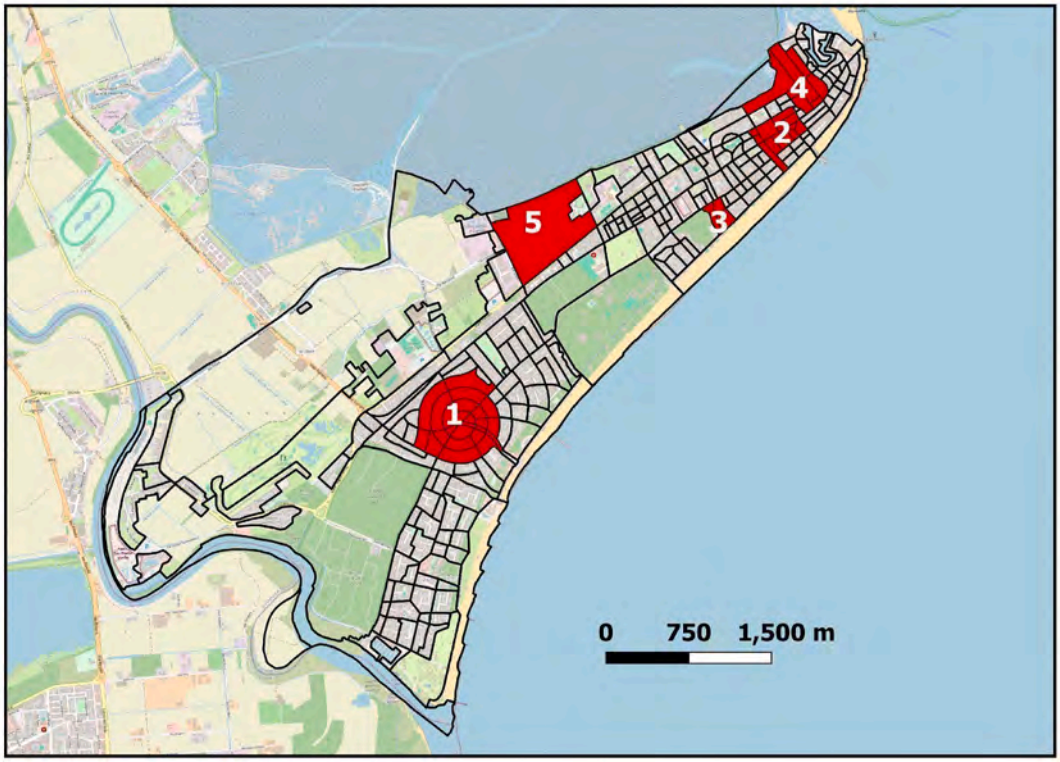

Fig. b.1. Location of the five target areas where visual validation activities were carried out in the Lignano municipality during July 2024, indicated by the red polygons.Validation stop points 1, 4 and 5 are illustrated in Figures B.2, B.3, and B.4. The black polygons represent the census units in Lignano. Background map data extracted from [26] is available at https://www.openstreetmap.org [91] and is licensed under the Open Data Commons Open Database License (ODbL).

Fig. b.2. An example of the newly constructed high-rise buildings in Lignano (a, b, and c), located at validation stop point number 2. Images in panel a and b are captured by the authors, c map data extracted from Google Earth engine (https://earthengine.google.com/) and d maps data extracted from [26] is available at https://www.openstreetmap.org [91] and is licensed under the Open Data Commons Open Database License (ODbL).

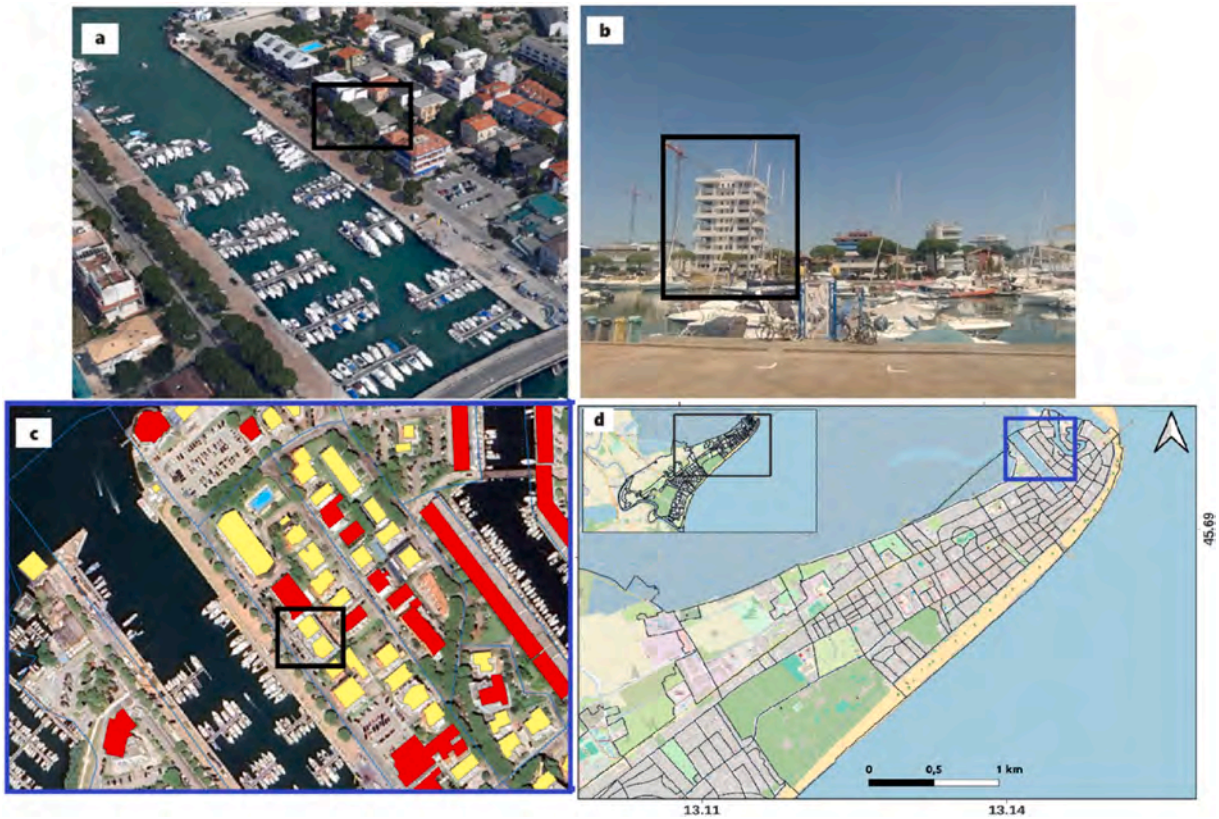

Fig. b.3. An example of replacing old low-rise single-family houses (a and c) with high-rise buildings (b) in Lignano, which is under construction as of July 2024. The building footprints (c) and Google Earth data (a) are outdated and still include the older low-rise single-family houses. Maps data a and c extracted from Google Earth engine (https://earthengine.google.com/) and d map data extracted from [26] is available at https://www.openstreetmap.org [91] and is licensed under the Open Data Commons Open Database License (ODbL). Image b is captured by the authors. Black rectangles pointing to the low-rise single-family houses (a and c) and high-rise buildings (b).

Fig. b.4. An example of the expansion of new building construction in rural areas. The blue polygon represents the census unit, which is comparatively coarser. Images a and b are captured by authors, and the lower map data extracted from [26] is available at https://www.openstreetmap.org [91] and is licensed under the Open Data Commons Open Database License (ODbL).

Data availability statement

High-resolution Population Density Maps is available athttps://dataforgood.facebook.com/dfg/. The census buildings data and the population census data are available for the years 2011 and 2021 from the census database [61,75] respectively. The digital building footprints are derived from the [77] (Eaglefvg - Sistema di consultazione delle banche dati territoriali della Regione Autonoma Friuli Venezia Giulia). The replacement cost is obtained from the last updated Real Estate Agency market values, provided by the Italian government for the year 2023 (agenziaentrate.gov.it).

References

[1] R. Figueiredo, M. Martina, Using open building data in the development of exposure data sets for catastrophe risk modelling, Nat. Hazards Earth Syst. Sci. 16 (2) (2016) 417–429, https://doi.org/10.5194/nhess-16-417-2016.
[2] G. Tocchi, M. Polese, M. Di Ludovico, A. Prota, Regional based exposure models to account for local building typologies, Bull. Earthq. Eng. (2022) 1–36, https://doi.org/10.1007/s10518-021-01242-6.
[3] G. Tocchi, G. Cremen, C. Galasso, M. Polese, Development of a Multi-Risk Index for Italy: a Tool for Supporting Informed Decision Making on Disaster Risk Reduction Prioritisation, Trinity College Dublin, 2023, July.
[4] J. Dabbeek, V. Silva, Modeling the residential building stock in the Middle East for multi-hazard risk assessment, Nat. Hazards 100 (2020) 781–810, https://doi.org/10.1007/s11069-019-03842-7.
[5] J. Dabbeek, V. Silva, C. Galasso, A. Smith, Probabilistic earthquake and flood loss assessment in the Middle East, Int. J. Disaster Risk Reduct. 49 (2020) 101662, https://doi.org/10.1016/j.ijdrr.2020.101662.

[6] J.C. Gill, B.D. Malamud, Reviewing and visualizing the interactions of natural hazards, Rev. Geophys. 52 (2014) 680–722.
[7] G. Zuccaro, D. De Gregorio, M.F. Leone, Theoretical model for cascading effects analyses, Int. J. Disaster Risk Reduct. 30 (2018) 199–215, https://doi.org/10.1016/j.ijdrr.2018.04.019, 2018.
[8] M.C. De Ruiter, A. Couasnon, M.J.C. van den Homberg, J.E. Daniell, J.C. Gill, P.J. Ward, Why we can no longer ignore consecutive disasters, Earths Future 8 (3) (2020) e2019ef001425, https://doi.org/10.1029/2019EF001425.
[9] S. Hochrainer-Stigler, R.Š. Trogrlić, K. Reiter, P.J. Ward, M.C. de Ruiter, M.J. Duncan, S. Gottardo, Toward a framework for systemic multi-hazard and multi-risk assessment and management, iScience 26 (5) (2023), https://doi.org/10.1016/j.isci.2023.106736.
[10] Goda, K. Goda, T. Rossetto, N. Mori, S. Tesfamariam, Mega quakes: cascading earthquake hazards and compounding risks, Front. Built Environ. 4 (2018) 8, https://doi.org/10.3389/fbuil.2018.00008, 2018.
[11] A. Almutairi, M. Mourshed, R.F.M. Ameen, Coastal community resilience frameworks for disaster risk management, Nat. Hazards 101 (2) (2020) 595–630, https://doi.org/10.1007/s11069-020-03875-3.
[12] V. Silva, S. Brzev, C. Scawthorn, C. Yepes, J. Dabbeek, H. Crowley, A building classification system for multi-hazard risk assessment, International Journal of Disaster Risk Science 13 (2) (2022) 161–177, https://doi.org/10.1007/s13753-022-00400-x.
[13] M.C. De Ruiter, J.A. de Bruijn, J. Englhardt, J.E. Daniell, H. de Moel, P.J. Ward, The asynergies of structural disaster risk reduction measures: comparing floods and earthquakes, Earths Future 9 (1) (2021) e2020EF001531.
[14] P. Patel, T. Pathak, S. Joshi, Study and analysis of irregularities in RC buildings, in: Recent Trends in Civil Engineering: Select Proceedings of ICRACE 2021, Springer Nature Singapore, Singapore, 2022, pp. 157–169, https://doi.org/10.1007/978-981-19-4055-2_14.
[15] J.E. Meyers-Angulo, S. Martínez-Cuevas, J.M. Gaspar-Escribano, Classifying buildings according to seismic vulnerability using Cluster-ANN techniques: application to the city of Murcia, Spain, Bull. Earthq. Eng. 21 (7) (2023) 3581–3622, https://doi.org/10.1007/s10518-023-01671-5.
[16] M. Mason, E. Phillips, T. Okada, J. O'Brien, Analysis of damage to buildings following the 2010-11 Eastern Australia floods, Nat. Clim. Change Adapt. Res. Facil. (2012).
[17] G. Cremen, C. Galasso, J. McCloskey, Modelling and quantifying tomorrow's risks from natural hazards, Sci. Total Environ. 817 (2022) 152552, https://doi.org/10.1016/j.scitotenv.2021.152552.
[18] G. Cremen, C. Galasso, J. McCloskey, A. Barcena, M. Creed, M.E. Filippi, R. Gentile, L.T. Jenkins, M. Kalaycioglu, E.Y. Mentese, M. Muthusamy, K. Tarbali, R.Š. Trogrlić, A state-of-the-art decision-support environment for risk-sensitive and pro-poor urban planning and design inTomorrow's cities, Int. J. Disaster Risk Reduct. 85 (2023) 103400, https://doi.org/10.1016/j.ijdrr.2022.103400.
[19] K. Otárola, L. Iannacone, R. Gentile, C. Galasso, Multi-hazard life-cycle consequence analysis of deteriorating engineering systems, Struct. Saf. (2024) 102515, https://doi.org/10.1016/j.strusafe.2024.102515.
[20] K. Bhuyan, C. Van Westen, J. Wang, S.R. Meena, Mapping and characterising buildings for flood exposure analysis using open-source data and artificial intelligence, Nat. Hazards 119 (2) (2023) 805–835, https://doi.org/10.1007/s11069-022-05612-4.
[21] J.C. Gomez-Zapata, N. Brinckmann, S. Harig, R. Zafrir, M. Pittore, F. Cotton, A. Babeyko, Variable-resolution building exposure modelling for earthquake and tsunami scenario-based risk assessment. An application case in Lima, Peru, Nat. Hazards Earth Syst. Sci. (2021) 1–30, https://doi.org/10.5194/nhess-21-3599-2021.
[22] J.C. Gómez Zapata, M. Pittore, N. Brinckmann, J. Lizarazo-Marriaga, S. Medina, N. Tarque, F. Cotton, Scenario-based multi-risk assessment from existing single-hazard vulnerability models. An application to consecutive earthquakes and tsunamis in Lima, Peru, Nat. Hazards Earth Syst. Sci. 23 (2023) 2203–2228, https://doi.org/10.5194/nhess-23-2203-2023.
[23] C. Scaini, A. Tamaro, B. Adilkhan, S. Sarzhanov, V. Ismailov, R. Umaraliev, E. Faga, A new regionally consistent exposure database for Central Asia: population and residential buildings, Nat. Hazards Earth Syst. Sci. 24 (3) (2024) 929–945, https://doi.org/10.5194/nhess-24-929-2024.
[24] C.I. Nievas, M. Pilz, K. Prehn, D. Schorlemmer, G. Weatherill, F. Cotton, Calculating earthquake damage building by building: the case of the city of Cologne, Germany, Bull. Earthq. Eng. (2022), https://doi.org/10.1007/s10518-021-01303-w.
[25] J.C. Gómez Zapata, R. Zafrir, M. Pittore, Y. Merino, Towards a sensitivity analysis in seismic risk with probabilistic building exposure models: an application in valparaiso, Chile using ancillary open-source data and parametric ground motions, ISPRS Int. J. GeoInf. 11 (2022), https://doi.org/10.3390/ijgi11020113.
[26] OpenStreetMap (https://www.openstreetmap.org/#map=13/45.67109/13.12265/) (last access 28 February 2025).
[27] C. Geiß, P. Priesmeier, P. Aravena Pelizari, A.R. Soto Calderon, E. Schoepfer, T. Riedlinger, M. Villar Vega, H. Santa María, J.C. Gómez Zapata, M. Pittore, E. So, A. Fekete, H. Taubenböck, Benefits of global earth observation missions for disaggregation of exposure data and earthquake loss modeling: evidence from Santiago de Chile, Nat. Hazards 119 (2023) 779–804, https://doi.org/10.1007/s11069-022-056726.
[28] C. Geiß, J. Maier, E. So, E. Schoepfer, S. Harig, J.C. Gómez Zapata, Y. Zhu, Anticipating a risky future: long short-term memory (LSTM) models for spatiotemporal extrapolation of population data in areas prone to earthquakes and tsunamis in Lima, Peru, Nat. Hazards Earth Syst. Sci. 24 (2024) 1051–1064, https://doi.org/10.5194/nhess-24-1051-2024.
[29] C. Arrighi, M. Tanganelli, M.T. Cristofaro, V. Cardinali, A. Marra, F. Castelli, M. De Stefano, Multi-risk assessment in a historical city, Nat. Hazards (2022), https://doi.org/10.1007/s11069-021-05125-6.
[30] J.C. Gómez Zapata, M. Pittore, F. Cotton, H. Lilienkamp, S. Shinde, P. Aguirre, H. Santa María, Epistemic uncertainty of probabilistic building exposure compositions in scenario-based earthquake loss models, Bull. Earthq. Eng. 20 (5) (2022) 2401–2438, https://doi.org/10.1007/s10518-021-01312-9.
[31] H. Crowley, Earthquake risk assessment: present shortcomings and future directions, Perspect. Eur. Earthq. Eng. Seismol. 1 (2014) 515–532, https://doi.org/10.1007/978-3-319-07118-3_16.
[32] C. Corbane, U. Hancilar, D. Ehrlich, T. De Groeve, Pan-European seismic risk assessment: a proof of concept using the Earthquake Loss Estimation Routine (ELER), Bull. Earthq. Eng. 15 (2017) 1057–1083, https://doi.org/10.1007/s10518-016-9993-5.
[33] V. Silva, S. Akkar, J. Baker, P. Bazzurro, J.M. Castro, H. Crowley, M. Dolsek, C. Galasso, S. Lagomarsino, R. Monteiro, D. Perrone, Current challenges and future trends in analytical fragility and vulnerability modeling, Earthq. Spectra 35 (4) (2019) 1927–1952, https://doi.org/10.1193/042418EQS101O.
[34] E.Y. Menteşe, G. Cremen, R. Gentile, C. Galasso, M.E. Filippi, J. McCloskey, Future exposure modelling for risk-informed decision making in urban planning, Int. J. Disaster Risk Reduct. 90 (2023) 103651, https://doi.org/10.1016/j.ijdrr.2023.103651.
[35] K. Chen, J. McAneney, R. Blong, R. Leigh, L. Hunter, C. Magill, Defining area at risk and its effect in catastrophe loss estimation: a dasymetric mapping approach, Appl. Geogr. 24 (2) (2004) 97–117, https://doi.org/10.1016/j.apgeog.2004.03.005.
[36] A.H. Thieken, T. Petrow, H. Kreibich, B. Merz, Insurability and mitigation of flood losses in private households in Germany, Risk Anal.: Int. J. 26 (2) (2006) 383–395, https://doi.org/10.1111/j.1539-6924.2006.00741.x.
[37] S. Schneiderbauer, D. Ehrlich, Risk, hazard and people's vulnerability to natural hazards, Rev. Definitions, Concepts Data. Eur. Comm. Joint Res. Centre. EUR 21410 (2004) 40.
[38] L. Martins, V. Silva, A global database of vulnerability models for seismic risk assessment, in: 16th European Conference on Earthquake Engineering. Thessaloniki, Greece, 2018.
[39] H. Matsutomi, T. Sakakiyama, S. Nugroho, M. Matsuyama, Aspects of inundated flow due to the 2004 indian ocean tsunami, Coast. Eng. J. 48 (2006) 167–195, https://doi.org/10.1142/S0578563406001350.
[40] D. Dominey-Howes, M. Papathoma, Validating a tsunami vulnerability assessment model (the PTVA Model) using field data from the 2004 Indian Ocean tsunami, Nat. Hazards 40 (2007) 113–136, https://doi.org/10.1007/s11069-006-0007-9.
[41] M. Neubert, T. Naumann, J. Hennersdorf, J. Nikolowski, The geographic information system-based f lood damage simulation model HOWAD, J Flood Risk Manag 9 (2016) 36–49, https://doi.org/10.1111/jfr3.12109.
[42] J. Nicholas, G.D. Holt, D.G. Proverbs, Towards standardising the assessment of flood damaged proper ties in the UK, Struct. Surv. 19 (2001) 163–172, https://doi.org/10.1108/02630800110406667.
[43] P.J. Ward, B. Jongman, F.S. Weiland, A. Bouwman, R. van Beek, M.F. Bierkens, H.C. Winsemius, Assessing flood risk at the global scale: model setup, results, and sensitivity, Environ. Res. Lett. 8 (4) (2013) 044019.

[44] C. Yepes-Estrada, A. Calderon, C. Costa, H. Crowley, J. Dabbeek, M.C. Hoyos, L. Martins, N. Paul, A. Rao, V. Silva, Global building exposure model for earthquake risk assessment, Earthq. Spectra 39 (4) (2023) 2212–2235, https://doi.org/10.1177/87552930231194048.
[45] Facebook Connectivity Lab and Center for, International Earth Science Information Network – CIESIN – Columbia University Uzebekistan: high resolution population density maps + demographic estimates Humanitarian Data Exchange (HDX) repository. https://data.humdata.org/dataset/uzbekistan-high-resolution-population-density-maps-demographic-estimates-2024-7-July-2024.
[46] T. Ullah, S. Lautenbach, B. Herfort, M. Reinmuth, D. Schorlemmer, Assessing completeness of OpenStreetMap building footprints using MapSwipe, ISPRS Int. J. GeoInf. 12 (4) (2023) 143, https://doi.org/10.3390/ijgi12040143.
[47] M. Bossard, J. Feranec, J. Othell, CORINE Land Cover Technical Guide: Addendum 2000, 40, European Environment Agency, Copenhagen, 2000.
[48] Pooya Sarabandi, Anne S. Kiremidjian, Building inventory information extraction from remote sensing data and statistical models, in: Proceedings of the 14th World Conference on Earthquake Engineering, 2008.
[49] J.P.D. Albuquerque, B. Herfort, M. Eckle, The tasks of the crowd: a typology of tasks in geographic information crowdsourcing and a case study in humanitarian mapping, Remote Sens. 8 (10) (2016) 859, https://doi.org/10.3390/rs8100859.
[50] C. Scaini, B. Petrovic, A. Tamaro, L. Moratto, S. Parolai, Near-real-time damage estimation for buildings based on strong-motion recordings: an application to target areas in northeastern Italy, Seismol. Soc. Am. 92 (6) (2021) 3785–3800, https://doi.org/10.1785/0220200430.
[51] L.J. Oostwegel, T.E. Zadeh, D. Schorlemmer, From shelters to skyscrapers: a worldwide exploration of buildings and building types using volunteered geographic information and earth observation datasets (No. EGU24-14888), Copernicus Meetings (2024), https://doi.org/10.5194/egusphere-egu24-14888, 2024.
[52] S. Tyagunov, M. Pittore, M. Wieland, S. Parolai, D. Bindi, K. Fleming, J. Zschau, Uncertainty and sensitivity analyses in seismic risk assessments on the example of Cologne, Germany, Nat. Hazards Earth Syst. Sci. 14 (6) (2014) 1625–1640, https://doi.org/10.5194/nhess-14-1625-2014.
[53] N.A. Wardrop, W.C. Jochem, T.J. Bird, H.R. Chamberlain, D. Clarke, D. Kerr, L. Bengtsson, S. Juran, V. Seaman, A.J. Tatem, Spatially disaggregated population estimates in the absence of national population and housing census data, Proc. Natl. Acad. Sci. USA 115 (14) (2018) 3529–3537, https://doi.org/10.1073/pnas.1715305115.
[54] Y. Qiu, X. Zhao, D. Fan, S. Li, Y. Zhao, Disaggregating population data for assessing progress of SDGs: methods and applications, Int. J. Digit. Earth 15 (1) (2022) 2–29, https://doi.org/10.1080/17538947.2021.2013553.
[55] QGIS.org, QGIS Geographic Information System, QGIS Association, 2024. http://www.qgis.org.
[56] M. Rota, A. Penna, C.L. Strobbia, Processing Italian damage data to derive typological fragility curves, Soil Dynam. Earthq. Eng. 28 (10–11) (2008) 933–947.
[57] S. Brzev, C. Scawthorn, A.W. Charleson, L. Allen, M. Greene, K. Jaiswal, V. Silva, GEM Building Taxonomy, GEM Foundation, 2013. No. 2013-02), Version 2.0.
[58] A. Maramai, B. Brizuela, L. Graziani, The Euro-mediterranean tsunami catalogue, Ann. Geophys. (2014).
[59] A. Maramai, L. Graziani, B. Brizuela, Italian Tsunami Effects Database (ITED): the first database of tsunami effects observed along the Italian coasts, Nat. Hazards Earth Syst. Sci. Discuss. (2019) 1–21, https://doi.org/10.3389/feart.2021.596044.
[60] A. Maramai, L. Graziani, B. Brizuela, Italian Tsunami Effects Database (ITED): the first database of tsunami effects observed along the Italian coasts, Front. Earth Sci. 9 (2021) 596044, https://doi.org/10.3389/feart.2021.596044.
[61] Istat, 15° Censimento della popolazione e delle abitazioni 2011, National buildings census, Istituto Nazionale di Statistica, Rome,Italy, 2021 (in Italian).
[62] D. Slejko, G.B. Carulli, R. Nicolich, A. Rebez, A. Zanferrari, A. Cavallin, C. Doglioni, F. Carraro, D. Castaldini, V. Iliceto, E. Semenza, Seismotectonics of the Eastern Southern Alps: a review, Bollettino di Geofisica Teorica e Applicata 31 (1989) 109–136.
[63] G. Bressan, C. Barnaba, P.L. Bragato, A. Peresan, G. Rossi, S. Urban, Distretti sismici del Friuli Venezia Giulia, Boll. di Geofisica Teorica ed Applicata 60 (2019) S1–S74, https://doi.org/10.4430/bgta0300.
[64] A. Rovida, R. Camassi, P. Gasperini, M. Stucchi, Catalogo parametrico dei terremoti italiani. Tratto da, 2011.
[65] A. Cavallin, L. Broili, G. Carulli, B. Martinis, G. Mele, L. Siro, D. Slejko, Case history: Friuli earthquake, Geol. Appl. Idrogeol. 21 (1986) 1–82.
[66] A. Peresan, H.M. Hassan, Scenario-based tsunami hazard assessment for Northeastern Adriatic coasts, Mediterr. Geosci. Rev. (2024) 1–24, https://doi.org/10.1007/s42990-024-00114-w.
[67] E. Xhafaj, H.M. Hassan, C. Scaini, A. Peresan, Simulation of large plausible tsunami scenarios associated with the 2019 Durres (Albania) earthquake source and adjacent seismogenic zones, Mediterr. Geosci. Rev. (2024) 1–21, https://doi.org/10.1007/s42990-024-00122-w.
[68] D. Camuffo, C. Secco, P. Brimblecombe, J. Martin-Vide, Sea storms in the Adriatic Sea and the Western mediterranean during the last millennium, Clim. Change 46 (1) (2000) 209–223, https://doi.org/10.1023/A:1005607103766.
[69] J. Šepić, I. Vilibić, N. Strelec Mahović, Northern Adriatic meteorological tsunamis: observations, link to the atmosphere, and predictability, J. Geophys. Res.: Oceans 117 (C2) (2012), https://doi.org/10.1029/2011JC007608.
[70] J. Šepić, I. Vilibić, I. Fine, Northern Adriatic meteorological tsunamis: assessment of their potential through ocean modeling experiments, J. Geophys. Res.: Oceans 120 (4) (2015) 2993–3010.
[71] I. Međugorac, M. Pasarić, Z. Pasarić, M. Orlić, Two recent storm-surge episodes in the Adriatic, Flood Risk Manag. Response 135 (2016).
[72] A. Maramai, B. Brizuela, L. Graziani, A database for tsunamis and meteotsunamis in the Adriatic Sea, Appl. Sci. 12 (11) (2022) 5577, https://doi.org/10.3390/app12115577.
[73] A. Trigila, C. Iadanza, M. Bussettini, B. Lastoria, Dissesto idrogeologico in Italia: pericolosità e indicatori di rischio. Edizione 2018, ISPRA, 2018, pp. 287–2018. Rapporti.
[74] C. Da Lio, L. Tosi, Land subsidence in the Friuli Venezia Giulia coastal plain, Italy: 1992–2010 results from SAR-based interferometry, Sci. Total Environ. 633 (2018) 752–764, https://doi.org/10.1016/j.scitotenv.2018.03.244.
[75] Istat, 15° Censimento della popolazione e delle abitazioni 2011, National buildings census, Istituto Nazionale di Statistica, Rome,Italy, 2011 (in Italian).
[76] V. Poggi, C. Scaini, L. Moratto, G. Peressi, P. Comelli, P.L. Bragato, S. Parolai, Rapid damage scenario assessment for earthquake emergency management, Seismol Res. Lett. 92 (4) (2021) 2513–2530, https://doi.org/10.1785/0220200245.
[77] Carta Tecnica Regionale Numerica (Eaglefvg - Sistema di consultazione delle banche dati territoriali della Regione Autonoma Friuli Venezia Giulia) (https://eaglefvg.regione.fvg.it/) (last access 7 July 2024).
[78] Osservatorio del Mercato Immobiliare - OMI) of the Italian revenue agency, 2023. https://www.agenziaentrate.gov.it/portale/web/guest/schede/fabbricatiterreni/omi/banche-dati/quotazioni-immobiliari (Accessed 7 July 2024).
[79] H. Crowley, V. Despotaki, S. Rodrigues, V. Silva, D. Toma-Danila, E. Riga, A. Karatzetzou, S. Fotopoulou, A. Zugic, L. Sousa, S. Ozcebe, P. Gamba, Exposure model for European seismic risk assessment, Earthq. Spectra 36 (2020) 875529302091942, https://doi.org/10.1177/8755293020919429, 2020.
[80] Pittore and working group, Risk-oriented taxonomy and ontology of urban subsystems and functional models, DV 5 (2.1) (2023).
[81] M. Mouhine, E. Hilali, Effect of setback irregularity location on the performance of RC building frames under seismic excitation, Arch. Civ. Eng. 66 (4) (2020), https://doi.org/10.24425/ace.2020.135228.
[82] G. Smiroldo, M. Fasan, C. Amadio, Fragility curves for reinforced concrete frames characterised by different regularity, Procedia Struct. Integr. 44 (2023) 283–290, https://doi.org/10.1016/j.prostr.2023.01.037.
[83] J. Behrens, F. Løvholt, F. Jalayer, S. Lorito, M.A. Salgado-Gálvez, M. Sørensen, E. Vyhmeister, Probabilistic tsunami hazard and risk analysis: a review of research gaps, Front. Earth Sci. 9 (2021) 628772, https://doi.org/10.3389/feart.2021.628772.
[84] C. Petrone, T. Rossetto, M. Baiguera, C. De la Barra Bustamante, I. Ioannou, Fragility functions for a reinforced concrete structure subjected to earthquake and tsunami in sequence, Eng. Struct. 205 (2020) 110120, https://doi.org/10.1016/j.engstruct.2019.110120.
[85] C. Scaini, B. Petrovic, C. Barnaba, A. Peresan, Engaging diverse stakeholders in exposure data collection: participatory tools and activities, Int. J. Disaster Risk Reduct. 119 (2025) 105179, https://doi.org/10.1016/j.ijdrr.2025.105179.
[86] R. Paulik, C. Zorn, L. Wotherspoon, J. Sturman, Modelling national residential building exposure to flooding hazards, Int. J. Disaster Risk Reduct. 94 (2023) 103826, https://doi.org/10.1016/j.ijdrr.2023.103826.

[87] H. Badreldin, H. M. Hassan, F. Romanelli, M. El-Hadidy, M.N. ElGabry, Joint multi-scenario-based earthquake and tsunami hazard assessment for Alexandria, Egypt, Appl. Sci. 14 (24) (2024) 11896, https://doi.org/10.3390/app142411896.
[88] A. Peresan, C. Scaini, C. Barnaba, Crowd-sourced buildings data collection and remote training: new opportunities to engage students in seismic risk reduction, Earth Sci., Syst. Soc. 3 (2023) 10088, https://doi.org/10.3389/esss.2023.10088.
[89] Y. Zhang, Z. Ouyang, C. Xu, T. Wu, F. Lu, A multi-hazard framework for coastal vulnerability assessment and climate-change adaptation planning, Environ. Sustain. Indicat. 21 (2024) 100327, https://doi.org/10.1016/j.indic.2023.100327.
[90] C. Chen, C. Peng, N.A.K. Nandasena, H. Yan, Experimental investigation on tsunami impact reduction on a building by a Mangrove Forest, Estuar. Coast Shelf Sci. 301 (2024) 108756, https://doi.org/10.1016/j.oceaneng.2023.114638.
[91] OpenStreetMap contributors, Planet Dump, Data licensed under the Open Data Commons Open Database License (ODbL) by the OpenStreetMap Foundation (OSMF), 2024. https://planet.openstreetmap.org. (Accessed 1 July 2024).